Variational quantum algorithm for generalized eigenvalue problems and its application to the finite-element method

Yuki Sato [1,2,*] Hiroshi C. Watanabe [2,3] Rudy Raymond [4,2,5] Ruho Kondo [1,2] Kaito Wada [6]
Katsuhiro Endo [7,2] Michihiko Sugawara [2] and Naoki Yamamoto [2,6]

[1]*Toyota Central R&D Labs., Inc., 41-1, Yokomichi, Nagakute, Aichi 480-1192, Japan*
[2]*Quantum Computing Center, Keio University, 3-14-1 Hiyoshi, Kohoku-ku, Yokohama, Kanagawa 223-8522, Japan*
[3]*Department of Chemistry, Graduate School of Science, Kyushu University, 744 Motooka, Nishi-ku, Fukuoka 819-0395, Japan*
[4]*IBM Quantum, IBM Japan, 19-21 Nihonbashi Hakozaki-cho, Chuo-ku, Tokyo 103-8510, Japan*
[5]*Department of Computer Science, The University of Tokyo, 7-3-1, Hongo, Bunkyo-ku, Tokyo 113-0033, Japan*
[6]*Department of Applied Physics and Physico-Informatics, Keio University, Hiyoshi 3-14-1, Kohoku-ku, Yokohama 223-8522, Japan*
[7]*Research Center for Computational Design of Advanced Functional Materials, National Institute of Advanced Industrial Science and Technology (AIST), 1-1-1 Umezono, Tsukuba, Ibaraki 305-8568, Japan*

Generalized eigenvalue problems (GEPs) play an important role in the variety of fields including engineering, machine learning, and quantum chemistry. Especially, many problems in these fields can be reduced to finding the minimum or maximum eigenvalue of GEPs. One of the key problems to handle GEPs is that the memory usage and computational complexity explode as the size of the system of interest grows. This paper aims at extending sequential quantum optimizers for GEPs. Sequential quantum optimizers are a family of algorithms that iteratively solve the analytical optimization of single-qubit gates in a coordinate descent manner. The contribution of this paper is as follows. First, we formulate the GEP as the minimization or maximization problem of the fractional form of the expectations of two Hermitians. We then show that the fractional objective function can be analytically minimized or maximized with respect to a single-qubit gate by solving a GEP of a 4×4 matrix. Second, we show that a system of linear equations characterized by a positive-definite Hermitian can be formulated as a GEP and thus be attacked using the proposed method. Finally, we demonstrate two applications to important engineering problems formulated with the finite-element method. Through the demonstration, we have the following bonus finding; a problem having a real-valued solution can be solved more effectively using quantum gates generating a complex-valued state vector, which demonstrates the effectiveness of the proposed method.

I. INTRODUCTION

Generalized eigenvalue problems (GEPs) are expressed as

$$A\boldsymbol{v} = \lambda B\boldsymbol{v}, \qquad (1)$$

where A and B are Hermitian matrices; also λ and $\boldsymbol{v}$ are the generalized eigenvalue and generalized eigenvector, respectively. GEPs play an important role in the variety of fields, including engineering [1], machine learning [2], and quantum chemistry [3]. In the field of engineering, finding the lowest eigenvalue of a symmetric generalized eigenvalue problem often appears in the finite-element approximation of mechanical structures to estimate their dynamical properties [4]. Many problems in machine learning can be reduced to finding the minimum or maximum eigenvalue of (generalized) eigenvalue problems, such as for the principal component analysis, canonical correlation analysis, and Fisher discriminant analysis [2]. A key problem is that, as the size of the system grows, memory usage and computational complexity explode. Actually, many works have been performed using

supercomputers to deal with the system with several tens of billion degrees of freedom [5,6].

Quantum computing is a promising and attractive approach to realize high-performance computing that is significantly faster than classical computing thanks to the capability of handling an exponentially large Hilbert space. For fault-tolerant quantum computers, the quantum phase estimation algorithm, which can be used to calculate the ground state of a system Hamiltonian in quantum chemistry [7,8], has already been applied to generalized eigenvalue problems [9]. Meanwhile, for near-term quantum computers, the variational quantum eigensolver (VQE) [10,11], which calculates the minimal eigenvalue of a Hamiltonian based on a classical-quantum hybrid scheme, has been extensively studied, especially for quantum chemistry [12,13]. VQE is a kind of the variational quantum algorithm (VQA) [14,15], where a certain function of expectation values of observables is minimized or maximized through a parametrized quantum circuit (PQC) or simply an *ansatz*. VQAs have been applied to various problems, including ground-state calculations [10,11,13,16], excited-state calculations [17–20], time-evolution simulations [21,22] for chemical calculations, partial differential equation solvers [23–25], algebraic operations such as linear

*yuki-sato@mosk.tytlabs.co.jp

system solvers [26,27], and principal component analysis [28,29]. VQAs have also been applied to generalized eigenvalue problems [30,31], where the cost function derived from the generalized Rayleigh quotient is optimized based on the gradient-based optimizer.

The sequential quantum optimizers are a family of algorithms which iterate the analytical optimizations of single-qubit gates in a coordinate descent manner. This concept was first studied in Ref. [32], proposing the sequential optimizer of single-qubit gates in the PQC, particularly their rotation angles; we call this method the Nakanishi-Fujii-Todo (NFT) algorithm. ROTOSOLVE [33], which was proposed independently from NFT, also optimizes the angle of a single-qubits gate, and ROTOSELECT [33], which was proposed together with ROTOSOLVE, optimizes the rotational angles of single-qubit gates selecting the optimal axes from a finite discrete set of axes. These methods were extended to the continuous optimization of rotational axes, which are called the "free-axis selection" (FRAXIS) [34] and the maximum optimization of a single-qubit gate termed "free-quaternion selection"(FQS) [35]. The methods exhibited better convergences compared with the gradient-based approaches [32,35] and a recent finding suggested that their behaviors with regards to the so-called *barren plateaus* are similar to their gradient-based counterparts [35]. These methods are applicable to several problems such as general VQE and simulation for real- or imaginary-time evolutions, but they are limited to the case where the objective function is in the form of the expectation of a problem Hamiltonian. In our case focusing on the GEPs in Eq. (1), unfortunately, A must be identity; that is, the GEPs could not be solved in the same way as the aforementioned methods.

In this paper, we extend the VQA based on the sequential quantum optimizers, in particular focusing on FQS [35], to solve GEPs characterized by two symmetric (more generally Hermitian) matrices.

The contributions of this paper are as follows. First, we reformulate the GEPs by the minimization or maximization problem of the generalized Rayleigh quotient, which is further reformulated in the fractional form of the expectations of two Hamiltonians as the objective function of the VQA. We then show that the sequential quantum optimization method is applicable; that is, the objective function can be analytically minimized or maximized with respect to a single-qubit gate by solving a GEP of a 4×4 matrix.

Second, we deal with the general problem of solving a system of linear equations (SLE), where an efficient solver is in great demand, e.g., for solving partial differential equations (PDE) [36], and in machine learning [37,38]. We show that the SLE problem, which is characterized by a positive-definite Hermitian, can be formulated in a form of GEP and thus be attacked using the proposed variational approach mentioned above. While several studies [23,24,39] have already applied VQAs to solving an SLE derived from PDEs, the proposed method is advantageous with respect to less controlled-unitary gates and auxiliary qubits required owing to expressing an SLE as a GEP.

Finally, we demonstrate two applications to engineering problems of importance formulated with the finite-element method [4,40]. One of the problems is for solving an SLE derived from a Poisson equation, and the other is eigenfre-

quency analysis of a beam structure. Based on these results, we give an estimate that a few dozen of qubits are required to solve practical problems. Through the demonstration, we have the following bonus finding; a problem having a real-valued solution can be solved more effectively using quantum gates generating a complex-valued state vector.

The rest of this paper is organized as follows. In Sec. II, we briefly discuss the GEP, which can be solved by minimizing or maximizing the generalized Rayleigh quotient. We also give an overview of sequential quantum optimizer, which optimizes a PQC in a coordinate descent manner. In Sec. III, we construct the method to fully minimize the generalized Rayleigh quotient with respect to a single-qubit gate by extending the FQS. We also give a VQA for solving an SLE in the GEP formulation. Section IV shows the two demonstrations. Finally, we conclude this study in Sec. V.

II. PRELIMINARIES

A. Generalized eigenvalue problem

In this paper, we focus on the minimum eigenvalue of the generalized eigenvalue problem (GEP) in Eq. (1), assuming that $B \in \mathbb{C}^{N \times N}$ is a positive-definite Hermitian matrix and $A \in \mathbb{C}^{N \times N}$ is a Hermitian matrix. To this end, it is convenient to introduce the generalized Rayleigh quotient R defined as

$$R(\boldsymbol{w}; A, B) := \frac{\boldsymbol{w}^{\dagger} A \boldsymbol{w}}{\boldsymbol{w}^{\dagger} B \boldsymbol{w}}, \tag{2}$$

where $\boldsymbol{w}$ is an arbitrary unit vector in $\mathbb{C}^N$. The minimum eigenvalue of the GEP (1) is identical to the minimum value of the generalized Rayleigh quotient R. Also, the minimizer $\boldsymbol{w}$ of R is identical to the eigenvector $\boldsymbol{v}$ corresponding to the minimum eigenvalue as explained in Appendix A. When one is interested in the maximum eigenvalue, it is enough to replace the minimum with the maximum over the following discussion.

B. Overview of sequential quantum optimizers

As an optimizer of PQC, this study employs a coordinate descent sequential optimizer which sequentially optimizes single-qubit gates in a PQC. The reasons to employ the sequential optimizers, in addition to their analytically computable solutions, are their better convergences [15,32,34,35] and a recent finding that their behaviors with regards to the so-called barren plateau are similar to their gradient-based counterparts [35]. Here, we give an overview of sequential quantum optimizers, especially FQS [35].

Let ρ denote a quantum state prepared through a PQC from an initial state ρ_0 as follows:

$$\rho = U_D \ldots U_d \ldots U_1 \rho_0 U_1^{\dagger} \ldots U_d^{\dagger} \ldots U_D^{\dagger}, \tag{3}$$

where D is the number of parametrized single-qubit gates and U_d ($d = 1, \ldots, D$) is the dth parametrized single-qubit gate. We herein omit representing fixed unitary gates that include nonlocal gates. Now, we represent the dth parametrized single-qubit gate U_d as

$$U_d := \boldsymbol{q}_d \cdot \vec{\varsigma}, \tag{4}$$

where

$$\boldsymbol{q}_d = \begin{pmatrix} \cos\left(\frac{\theta_d}{2}\right) \\ \sin\left(\frac{\theta_d}{2}\right)n_{dx} \\ \sin\left(\frac{\theta_d}{2}\right)n_{dy} \\ \sin\left(\frac{\theta_d}{2}\right)n_{dz} \end{pmatrix}, \tag{5}$$

and $\vec{\varsigma} = (I, -\iota X, -\iota Y, -\iota Z)$ with ι the imaginary unit and X, Y, and Z the Pauli matrix. θ_d and $\boldsymbol{n}_d = (n_{dx}, n_{dy}, n_{dz})$ are the rotational angle and axis of the dth gate, respectively. That is, U_d is parametrized by the unit quaternion $\boldsymbol{q}_d$. Accordingly, the quantum state is parametrized with the set of $\{\boldsymbol{q}_d\}_{d=1}^{D}$ as $\rho = \rho(\{\boldsymbol{q}_d\}_{d=1}^{D})$. The strategy of sequential optimization is to repeat the exact optimization of $\boldsymbol{q}_d$ for all $d = 1, \ldots, D$. Actually, the expectation $\langle H \rangle$ can be expressed as the quadratic form of the unit quaternion $\boldsymbol{q}_d$ as follows:

$$\langle H \rangle(\boldsymbol{q}_d) = \boldsymbol{q}_d^\top S(\rho', H')\boldsymbol{q}_d, \tag{6}$$

where

$$\rho' = U_{d-1}\ldots U_1\rho_0 U_1^\dagger \ldots U_{d-1}^\dagger, \tag{7}$$

$$H' = U_{d+1}^\dagger \ldots U_D^\dagger H U_D \ldots U_{d+1}, \tag{8}$$

and $S(\rho', H')$ is a 4×4 real symmetric matrix whose (i, j) component is defined as

$$(S)_{ij} := \tfrac{1}{2}\mathrm{tr}[\rho'(\varsigma_i^\dagger H' \varsigma_j + \varsigma_j^\dagger H' \varsigma_i)], \tag{9}$$

and can be constructed from expectation values of H calculated using 10 parameter sets, which we call *parameter configuration* [41]. The minimizer of $\langle H \rangle(\boldsymbol{q}_d)$ is the eigenvector corresponding to the minimum eigenvalue of the following eigenvalue problem of the 4×4 matrix $S(\rho', H')$:

$$S(\rho', H')\boldsymbol{q}_d = \lambda\boldsymbol{q}_d, \tag{10}$$

where λ is an eigenvalue. Thus, FQS gives the exact minimizer of the objective function $\langle H \rangle$ with respect to $\boldsymbol{q}_d$, by solving the above eigenvalue problem.

Because the FQS formulation gives a unified form of sequential quantum optimizer of PQCs [35], other sequential quantum optimizers can also be reduced to an eigenvalue problem. In NFT [32] (also in ROTOSOLVE [33]), the angle around a fixed axis $\boldsymbol{n}$ of a single-qubit gate serves as the parameter. That is, the parametrized single-qubit gate U_d is represented as

$$U_d = \boldsymbol{q}_d \cdot \vec{\varsigma} = \cos\left(\frac{\theta_d}{2}\right)I - \iota\sin\left(\frac{\theta_d}{2}\right)\boldsymbol{n}\cdot\vec{\sigma}, \tag{11}$$

where $\vec{\sigma} = (X, Y, Z)$, and the quaternion $\boldsymbol{q}_d$ is now restricted to $\left(\cos(\theta_d/2), \sin(\theta_d/2)\boldsymbol{n}^\top\right)^\top$. Then, the expectation $\langle H \rangle$ can be written as the quadratic form of the vector $\boldsymbol{c}_d := \left(\cos(\theta_d/2), \sin(\theta_d/2)\right)^\top$, as follows [35]:

$$\langle H \rangle(\boldsymbol{c}_d) = \boldsymbol{c}_d^\top \begin{bmatrix} S_{00} & \vec{S}_0 \cdot \boldsymbol{n} \\ \vec{S}_0 \cdot \boldsymbol{n} & \boldsymbol{n}^\top \tilde{S}\boldsymbol{n} \end{bmatrix}\boldsymbol{c}_d, \tag{12}$$

where $\vec{S} := (S_{01}, S_{02}, S_{03})$ and $\tilde{S}$ is the 3×3 matrix consisting of the lower right components of S. NFT minimizes the objective function $\langle H \rangle$ with respect to the angle of a single-qubit gate, through the eigenvalue problem of the matrix in Eq. (12).

In ROTOSELECT [33], a finite discrete set of axes is prepared and the angle of the single-qubit gate is tried to be updated with respect to each axis in the set by using NFT. Then, the angle and axis that give the minimum objective function are selected. Thus, ROTOSELECT adjusts the axis of the single-qubit gates in a discrete way. In FRAXIS [34], the axis of a single-qubit gate is to be optimized under the condition that its angle is fixed to a constant (typically, π). That is, the parametrized single-qubit gate U_d is represented as

$$U_d = \boldsymbol{q}_d \cdot \vec{\varsigma} = -\iota\boldsymbol{n}_d \cdot \vec{\sigma}. \tag{13}$$

The quaterinion $\boldsymbol{q}_d$ is now restricted to $(0, \boldsymbol{n}_d)^\top$. Then, the expectation $\langle H \rangle$ can be written as the quadratic form of the vector $\boldsymbol{n}_d$, as follows [34]:

$$\langle H \rangle(\boldsymbol{n}_d) = \boldsymbol{n}_d \tilde{S}\boldsymbol{n}_d. \tag{14}$$

FRAXIS minimizes the objective function of the form $\langle H \rangle$ with respect to the axis of a single-qubit gate through the eigenvalue problem of the 3×3 matrix $\tilde{S}$.

To solve the eigenvalue problem, the FQS formulation requires solving a quartic equation to obtain the (local) optimal gate, while the FRAXIS and NFT require, respectively, solving a cubic and a quadratic equation. All of these equations for FQS, FRAXIS, and NFT can be solved analytically [42].

III. METHOD

A. Extension of FQS to fractional objective function

The problem of finding the minimum eigenvalue of Eq. (1) is reduced to minimization of the generalized Rayleigh quotient (2). Here we take the approach using a quantum computer to solve this problem; then $\boldsymbol{w} \in \mathbb{C}^N$ in Eq. (2) is replaced with a quantum state vector $|\psi\rangle$ of n-qubit system, and the generalized Rayleigh quotient is expressed as

$$\mathcal{F}(\rho) := \frac{\mathrm{tr}(A\rho)}{\mathrm{tr}(B\rho)}, \tag{15}$$

where $\rho = |\psi(\{\boldsymbol{q}_d\}_{i=d}^{D})\rangle\langle\psi(\{\boldsymbol{q}_d\}_{d=1}^{D})|$. Note that the required number of qubits is $O(\log_2 N)$, which is thus the advantage of using quantum computation. If $\log_2 N$ is not an integer, the matrices A and B can be modified so that their dimensions become $2^n \times 2^n$ where $n = \lceil\log_2 N\rceil$ as discussed in Appendix B.

In the formulation of sequential quantum optimization to repeatedly optimize $\boldsymbol{q}_d$, the expectations can be expressed as Eq. (6), and thus Eq. (15) is rewritten as

$$\mathcal{F}(\boldsymbol{q}_d) = \frac{\boldsymbol{q}_d^\top S(\rho', A')\boldsymbol{q}_d}{\boldsymbol{q}_d^\top S(\rho', B')\boldsymbol{q}_d}, \tag{16}$$

where $\boldsymbol{q}_d$ is the single-parameter vector (5). Also $S(\rho', A')$ and $S(\rho', B')$ are the matrices whose components are calculated by Eq. (9) for A and B, respectively. Because Eq. (16) takes the same form as the Rayleigh quotient (2), $\mathrm{argmin}_{\boldsymbol{q}_d}\mathcal{F}(\boldsymbol{q}_d)$ is identical to the eigenvector corresponding to the minimum eigenvalue of the following four-dimensional GEP:

$$S(\rho', A')\boldsymbol{p}_i = \lambda_i S(\rho', B')\boldsymbol{p}_i, \tag{17}$$

Algorithm 1 Sequential optimizer for fractional objective function.

Input: PQC structure, Hermitians A and B, tolerance ε_{tol}.
Output: Optimized parameters $\{\boldsymbol{q}_d^*\}_{d=1}^D$.
1: Set initial parameters $\{\boldsymbol{q}_d\}_{d=1}^D$ randomly.
2: Set $\mathcal{F}_{\text{curr}} \leftarrow 0$, $\mathcal{F}_{\text{prev}} \leftarrow 0$, $\varepsilon \leftarrow 1$
3: **while** $\varepsilon > \varepsilon_{\text{tol}}$ **do**
4:    **for** d in $[1, D]$ **do**
5:        Construct the matrix $S(\rho', A')$ and $S(\rho', B')$.
6:        Update $\boldsymbol{q}_d$ by solving Eq. (17).
7:        Set $\mathcal{F}_{\text{prev}} \leftarrow \mathcal{F}_{\text{curr}}$
8:        Set $\mathcal{F}_{\text{curr}} \leftarrow \lambda$
               $\triangleright$ λ is the minimum or maximum eigenvalue.
9:        Set $\varepsilon \leftarrow \|\mathcal{F}_{\text{curr}} - \mathcal{F}_{\text{prev}}\| / \|\mathcal{F}_{\text{prev}}\|$
10: **return** $\{\boldsymbol{q}_d\}_{d=1}^D$

---

where λ_i is the ith eigenvalue and $\boldsymbol{p}_i$ is the ith unit eigenvector. Assuming that the eigenvalues are indexed in the ascending order, $\min_{\boldsymbol{q}_d} \mathcal{F}(\boldsymbol{q}_d) = \lambda_1$ and $\operatorname{argmin}_{\boldsymbol{q}_d} \mathcal{F}(\boldsymbol{q}_d) = \boldsymbol{p}_1$.

The entire procedure of the proposed method is shown in Algorithm 1. The parameters of the single-qubit gates in a PQC are sequentially updated by solving the GEP (17) until the value of the objective function becomes less than a given tolerance value ε_{tol}. In this study, the order of optimizing the single-qubit gates in line 4 in Algorithm 1 is simply chosen as the ascending order, i.e., from top left to bottom right in the circuit diagram of PQC. We call the procedure from line 3 to 9 in Algorithm 1 an *iteration*, which updates all single-qubit gates once.

Since the matrices $S(\rho', A')$ and $S(\rho', B')$ are constructed by expectation values of A and B, they will include the sampling errors, i.e., shot noises. Due to sampling errors, the matrix $S(\rho', B')$ can be no longer positive definite when the number of sampling is relatively small. This will cause the numerical instability in solving Eq. (17). Thus, if the minimum eigenvalue of $S(\rho', B')$, $\beta_{\min}$, is negative, we add $(\epsilon - \beta_{\min})I$ to $S(\rho', B')$ where ϵ is a small positive constant. This ensures that Eq. (17) is well posed although the update direction of parameters is slightly changed.

Let us assume that, through this sequential optimization, we find the set of parameters $\{\boldsymbol{q}_d^*\}_{d=1}^D$ that exactly minimizes $\mathcal{F}(\rho)$; this gives us the solution of GEP in the form of quantum state as $|\boldsymbol{v}\rangle = |\psi(\{\boldsymbol{q}_d^*\}_{i=d}^D)\rangle$. Note that $O(N)$ measurements are required to retrieve all the components from the quantum state $|\boldsymbol{v}\rangle$. Hence, as discussed in [43], the proposed method should be used in the case where only some characteristic quantities about the solution are of interest; typically, such quantity is represented by $\langle \boldsymbol{v}|M|\boldsymbol{v}\rangle$ with M a Hermitian matrix, which can thus be efficiently computed on a quantum computer. Actually, in Sec. IV, we provide two examples where this assumption makes sense from an engineering point of view.

Lastly, note that, because the FQS formulation gives a unified form of sequential optimizer of PQCs [35], other sequential approaches, such as NFT [32], ROTOSOLVE/ROTOSELECT [33], and FRAXIS [34], can also be applied to solve the GEP problem in the similar approach. We indeed use them to compare with FQS in the experiments.

B. Asymptotic behavior of a parameter update under sampling errors

We solve Eq. (17) to update parameters of a single-qubit gate. Since the matrix $S(\rho', A')$ and $S(\rho', B')$ include sampling errors under a finite number of shots, the resulting eigenvalues and eigenvectors will also include fluctuation. Here, we summarize the asymptotic behavior of eigenvalues of Eq. (17). We provide the detailed analysis in Appendix C. In the following, we consider the minimization of the objective function, i.e., the minimum eigenvalue of Eq. (17).

Let n_s be the number of shots per individual quantum circuit. Since $S(\rho', A')$ and $S(\rho', B')$ are, respectively, constructed by the linear combination of expectation values of A and B calculated by several parameter sets, their perturbations can be represented as

$$S(\rho', A') = S(\rho', A')^{(0)} + \epsilon S(\rho', A')^{(1)}, \tag{18}$$

$$S(\rho', B') = S(\rho', B')^{(0)} + \epsilon S(\rho', B')^{(1)}, \tag{19}$$

where ϵ is $O(1/\sqrt{n_s})$, the superscript (0) represents a quantity without any perturbation and (1) represents one with perturbation. By considering the second-order asymptotic expansion of eigenvalues λ_i and eigenvectors $\boldsymbol{p}_i$, we obtain

$$\mathbb{E}[\lambda_i] = \lambda_i^{(0)} + \epsilon^2 \lambda_i^{(0)} \mathbb{E}\big[\big(\boldsymbol{p}_i^{(0)\top} S(\rho', B')^{(1)} \boldsymbol{p}_i^{(0)}\big)^2\big]$$
$$- \epsilon^2 \mathbb{E}\big[\boldsymbol{p}_i^{(1)\top}\big(S(\rho', A')^{(0)} - \lambda_i^{(0)} S(\rho', B')^{(0)}\big)\boldsymbol{p}_i^{(1)}\big]. \tag{20}$$

Therefore, the estimation of the objective function value $\mathcal{F}$ by the minimum eigenvalue λ_i has the bias that vanishes asymptotically no slower than or equal to ϵ^2, i.e., $O(1/n_s)$. Similarly, we can estimate the objective function value after update of parameters using the perturbed eigenvector, as follows:

$$\mathbb{E}[\mathcal{F}(\boldsymbol{p}_1)]$$
$$\approx \lambda_1^{(0)} + \epsilon^2 \mathbb{E}\big[\boldsymbol{p}_1^{(1)\top}\big(S(\rho', A')^{(0)} - \lambda_1^{(0)} S(\rho', B')^{(0)}\big)\boldsymbol{p}_1^{(1)}\big]$$
$$\leqslant \lambda_1^{(0)} + \epsilon^2\big(\lambda_{\max}^{(0)} - \lambda_1^{(0)}\big)\mathbb{E}\big[\boldsymbol{p}_1^{(1)\top} S(\rho', B')^{(0)} \boldsymbol{p}_1^{(1)}\big], \tag{21}$$

where $\lambda_{\max}$ is the maximum eigenvalue. The second term is related to the magnitude of the imperfect parameter update due to sampling errors and vanishes asymptotically no slower than or equal to ϵ^2. This equation indicates that the magnitude of the imperfection depends on the difference between the maximum and minimum eigenvalues of Eq. (17), i.e., the maximum and minimum objective function values reachable by changing parameters of the single-qubit gate to be updated. Therefore, when the difference is large, the objective function after parameter update can become large, and vice versa.

C. Generalized eigenvalue problem for a system of linear equations

Here we consider a system of linear equations (SLE)

$$K\boldsymbol{u} = \boldsymbol{f}, \tag{22}$$

where $K \in \mathbb{C}^{N \times N}$ is a given positive-definite matrix, $\boldsymbol{u} \in \mathbb{C}^N$ is an unknown vector, and $\boldsymbol{f} \in \mathbb{C}^N$ is a given vector. Without loss of generality, we assume that $\|\boldsymbol{f}\| = 1$. Such SLE arises

in a variety of applications including partial differential equation [36] and machine learning [37,38].

The problem of solving the SLE can be formulated as a GEP as follows:

$$f f^{\dagger} v = \lambda K v, \qquad (23)$$

where $v \in \mathbb{C}^N$ is an eigenvector and $\lambda \in \mathbb{R}$ is the corresponding eigenvalue. Here, $f f^{\dagger}$ corresponds to A in Eq. (15). Since $f f^{\dagger}$ is a rank-1 matrix, this GEP has only one nonzero and nondegenerate eigenvalue; the other $N - 1$ eigenvalues are all zeros. Using the nonzero eigenvalue $\hat{\lambda}$ and the corresponding eigenvector $\hat{v}$, the GEP reads as

$$K \left(\frac{\hat{\lambda} \hat{v}}{f^{\dagger} \hat{v}} \right) = f. \qquad (24)$$

Since $\hat{\lambda}$ is the nonzero eigenvalue, it is ensured that $f^{\dagger} \hat{v} \neq 0$ from Eq. (23). Substituting Eq. (24) into (22), we obtain

$$K \left(u - \frac{\hat{\lambda} \hat{v}}{f^{\dagger} \hat{v}} \right) = 0. \qquad (25)$$

Since K is positive definite, i.e., invertible, we obtain

$$u = \frac{\hat{\lambda} \hat{v}}{f^{\dagger} \hat{v}}, \qquad (26)$$

meaning that the solution of the SLE is given by the nonzero (maximal) eigenvalue and its corresponding eigenvector of the GEP (23).

Therefore, we can employ a quantum computer to solve the SLE (22), by formulating it as the GEP (23) and using the method described in Sec. III A. That is, we represent f by a quantum state vector $|f\rangle$ of $\lceil \log_2 N \rceil$-qubit system, which leads to a GEP (1) with $A = |f\rangle\langle f|$ and $B = K$. Note that the expectation $\mathrm{tr}(A\rho) = \mathrm{tr}(|f\rangle\langle f|\rho)$ can be evaluated as the fidelity of ρ and $|f\rangle$. Let us assume that the algorithm described in Sec. III A yields the optimal $\{q_d\}$ and accordingly the optimal $|\psi(\{q_d\})\rangle = |\hat{v}\rangle$, which is the quantum-state representation of the optimal $\hat{v}$. This gives us the optimal $|u\rangle = u$ as well, if we are just interested in the solution up to the constant. Otherwise, to have the exact solution u, we additionally need to calculate the value of $f^{\dagger} \hat{v} = \langle f | \psi(\{q_d\}) \rangle$.

Note that, in contrast to the variational quantum algorithms for solving an SLE [23,26], the proposed method does not require any auxiliary qubit *during* the optimizing process of the PQC. A brief explanation is as follows. In Ref. [26], the auxiliary qubit is required to perform the Hadamard test and Hadamard-overlap test to update the parameters; also Ref. [23] needs to prepare the entangled state $(|0\rangle|f\rangle + |1\rangle|\psi\rangle)/\sqrt{2}$, with $|\psi\rangle$ the state generated by a PQC, in order to evaluate the inner product $\langle f|\psi \rangle$ and accordingly the cost for updating the parameters. On the other hand, as described above, the proposed method generates $\hat{v} = |\hat{v}\rangle$ without any auxiliary qubit. If one needs $u = |u\rangle$, the proposed method also requires an auxiliary qubit to calculate the inner product $f^{\dagger} \hat{v} = \langle f|\psi \rangle$ on the quantum device, but this operation is necessary only once after the entire optimization process.

D. Complexity and resource

Let us assume that A and B are band matrices with the bandwidth of k_A and k_B, respectively, which typically appear in the problem of finite-element method (FEM). The proposed method calculates the expectation values of A and B, which requires $O(nk)$ kinds of quantum circuits using the extended Bell measurement (XBM) technique [44], where $n = \lceil \log_2 N \rceil$ and $k := \max(k_A, k_B)$. An overview of XBM is given in Appendix D. Suppose the number of shots per quantum circuit is s. Then, the total number of shots required to calculate expectation values of A and B is $O(nks)$.

Also, as mentioned below Eq. (15), the proposed method has a quantum advantage that it uses only $\lceil \log_2 N \rceil$ qubits to represent a vector in $\mathbb{C}^N$. Thus, even for practical problems using the FEM with tens or hundreds of thousands of degrees of freedom [45–47], it requires only less than 20 qubits.

To encode the right-hand side vector f into a quantum state $|f\rangle$, we have to design the so-called *oracle* U_f that prepares $|f\rangle = U_f|0\rangle^{\otimes n}$. When f corresponds to a relatively simple input representing such as a point source or uniform input, the oracle can be intuitively designed using Pauli-X and Hadamard gates, as we describe in Sec. IV A 2. In general cases, on the other hand, some amplitude encoding techniques [48,49] are required.

IV. NUMERICAL EXPERIMENTS

In the following, we provide numerical experiments. Unless otherwise stated, we used the state-vector simulator of QISKIT [50].

A. Solving the Poisson equation

1. Problem statement

We apply the proposed method to the problem of solving a partial differential equation (PDE). Among PDEs, we here focus on the Poisson equation, which appears in versatile applications including steady-state heat transfer, electrostatics [51], and computational fluid dynamics [52,53]. Before proceeding, recall that the proposed method obtains the solution vector as a quantum state $|\psi\{q_d\}\rangle$, meaning that practically we can retrieve only a few characteristic quantities from it. For the case of PDE problem, such partial information is for instance the surface temperature of a material, which indeed can be calculated from a few components of the entire solution vector of the Poisson equation.

Let $\Omega \subset \mathbb{R}^m$ denote an open bounded set where m is the number of spatial dimensions. The Poisson equation governs the state field $u(x) \in \mathbb{C}$ at the spatial coordinate $x \in \Omega$, which behaves as

$$-\nabla^2 u(x) = f(x) \quad \text{for } x \in \Omega, \qquad (27)$$

where ∇ is the gradient operator with respect to x and $f(x) : \Omega \to \mathbb{C}$ is a given function. We impose the Dirichlet boundary condition on $\partial\Omega$ as

$$u(x) = 0 \quad \text{on } x \in \partial\Omega. \qquad (28)$$

Discretizing the Poisson equation by FEM [4,40] yields an SLE written as follows:

$$KU = F, \qquad (29)$$

where $K \in \mathbb{R}^{N \times N}$ is a positive-definite matrix called the stiffness matrix; also, $U \in \mathbb{C}^N$ and $F \in \mathbb{C}^N$ are the discretized vectors of $u(\boldsymbol{x})$ and $f(\boldsymbol{x})$, respectively. N is the number of nodes of the finite-element mesh. The discretization procedure by FEM is detailed in Appendix E 1.

The SLE (29) has the form of Eq. (22) and, thus, it can be formulated as a GEP and solved using a quantum computer. The procedure is summarized in Algorithm 1; in our case, $A = \boldsymbol{F}\boldsymbol{F}^\dagger$ and $B = K$. In particular, because K is a band matrix, the expectation value $\mathrm{tr}(B\rho) = \mathrm{tr}(K\rho)$ can be efficiently calculated by XBM [44]. Also, due to the linearity of Eq. (29), we can set $\|F\| = 1$ to well define the quantum state $|F\rangle$. Then, assuming that $|F\rangle$ is efficiently prepared by a unitary U_F, i.e., $|F\rangle = U_F |0\rangle^{\otimes n}$, we can use the inversion test [54] to calculate $\mathrm{tr}(A\rho) = \mathrm{tr}(|F\rangle\langle F|\rho)$.

Here, we focus on the one-dimensional Poisson equation discretized by the first-order elements whose lengths are uniformly 1. We use $32 = 2^5$ nodes for discretization, which requires 5 qubits. As a test case, we herein set the right-hand side of the Poisson equation, $f(\boldsymbol{x})$, to a step function given in the form of quantum state as

$$|F\rangle = \frac{1}{2^{n/2}} \sum_{j=0}^{N-1} (-1)^{j_{n-1}} |j\rangle, \qquad (30)$$

where j_{n-1} is the value of the most significant bit (MSB) of the unsigned binary representation of j. This quantum state $|F\rangle$ can be efficiently prepared by the the following unitary U_F:

$$U_F = H^{\otimes n}(X \otimes I^{\otimes(n-1)}). \qquad (31)$$

Note that, since $|F\rangle$ is a real vector in $\mathbb{R}^{2^n}$ and K is a real matrix, the solution of this problem also lies in the real space.

2. Results and discussion

(a) Dependency of results on initial parameters. This part shows the dependency of results on the initial parameters.

We applied the proposed method with FQS, FRAXIS, RO-TOSELECT, and NFT to solving the above-described Poisson equation. For NFT, we use the R_y gate $R_y(\theta) = e^{-i\theta Y}$ with Y the Pauli-Y matrix, for all parametrized single-qubit gates, where the angles of these gates are randomly initialized. For FRAXIS, the rotational axes of all single-qubit gates were set randomly on the unit spherical surface. For FQS and ROTOS-ELECT, we employed two initialization strategies termed the *real-space initialization* and the *complex-space initialization*. In the real-space initialization, the rotational axes of all single-qubit gates were set to y axis in the beginning of VQA, while their initial angles were randomly generated both for ROTOSELECT and FQS. In the complex space initialization for ROTOSELECT, the initial rotational axis of single-qubit gates was randomly selected from x, y, or z axes and the angles of the gates also randomly initialized. The complex-space initialization for FQS randomly set initial unit quaternions; that is, a quaternion is sampled uniformly from the three-dimensional
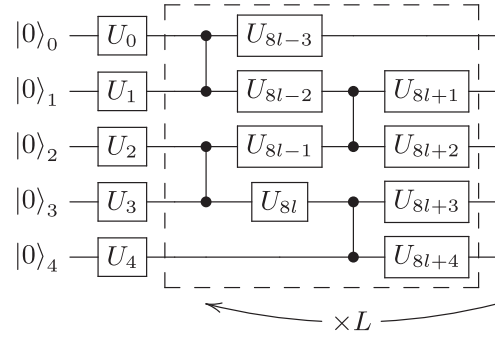

FIG. 1. Alternating layered PQC for five qubits.

unit hyper-sphere. We employed the alternating layered PQC [55] shown in Fig. 1 and set the number of layers to $L = 2$. The 30 independent trials with both initializations were performed to examine the statistical behaviors of the proposed method.

Figure 2 shows box plots of the relative errors of the resulting objective function value after optimization, compared to the exact minimum value $\mathcal{F}^*$. FQS with the complex-space initialization clearly exhibits better capability of obtaining lower objective function values, which implies that the use of complex space is effective even for problems involving the solution lying in the real space.

To comprehend the behaviors of searching in the complex space more clearly, we analyzed the distance of the state vector during the optimization process from the real space. Let r_i and c_i denote the real and imaginary parts of the ith complex amplitude of the state vector, respectively. When the state vector lies in the real space up to a global phase, all the points $\{(r_i, c_i)\}_{i=0}^{2^n-1}$ on the complex plane lie in a straight line. Thus, the distance from the state vector to the real space can be evaluated by the distance from the point set $\{(r_i, c_i)\}_{i=0}^{2^n-1}$ to a line. Let X be a matrix in $\mathbb{R}^{2^n \times 2}$ whose first and the second columns are $(r_0, \ldots, r_{2^n-1})^\top$ and $(c_0, \ldots, c_{2^n-1})^\top$, respectively. Then, the distance from the point set $\{(r_i, c_i)\}_{i=0}^{2^n-1}$ to a line in the complex plane can be calculated as the minimum eigenvalue of $X^\top X$ based on the principal component analysis (PCA). Using the two eigenvalues denoted by $\mu_1 > \mu_2$, we define the
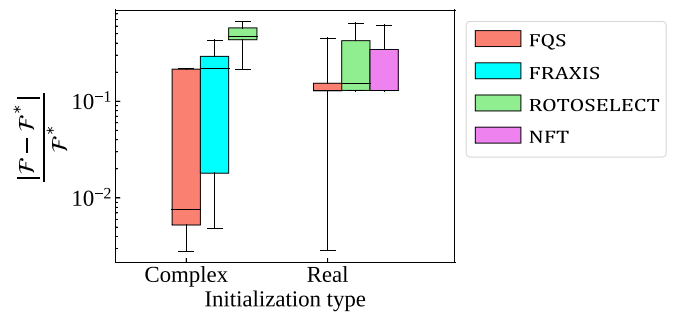

FIG. 2. Box plots of the relative error of the resulting objective function with respect to the exact minimum value $\mathcal{F}^*$. VQA were conducted on the alternating layered PQC of $L = 2$. The 30 independent trials were performed for each of the real- and the complex-space initialization methods.
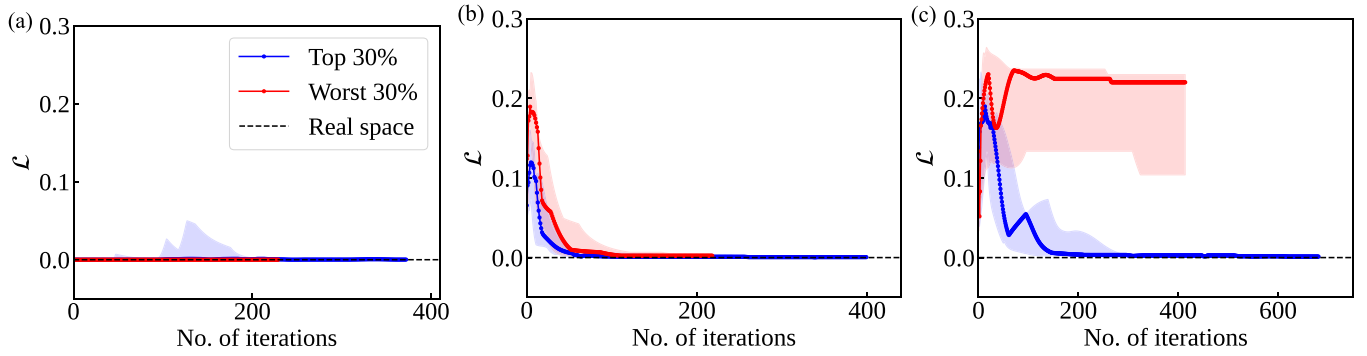
FIG. 3. The distance from the state vector to the real space for the result of (a) FQS with real-space initialization, (b) FQS with complex-space initialization, and (c) FRAXIS. The blue plots are the median values of the top 30% solutions among the 30 independent trials and the blue shaded ranges illustrate the 25th and 75th percentiles. The red plots are the median values of the worst 30% solutions among the trials and the red shaded regions represent the 25th and 75th percentiles.

metric of the distance from the state vector to the real space as

$$\mathcal{L} := \frac{\mu_2}{\mu_1 + \mu_2}. \tag{32}$$

Figure 3 shows the histories of the distance $\mathcal{L}$ of the state vector during the optimization by FQS and FRAXIS for the top 30% and the worst 30% trials among 30 trials in terms of the resulting objective function values. Note that the number of iterations until convergence is not necessarily consistent among 30 trials. Hence, we completed the shorter trajectories by the final value at the last iteration such that the lengths of the trajectories were equalized. As shown in Fig. 3(a), the top 30% trials starting from the real-space initialization used the complex space in optimization process, while the states of the worst 30% trials stayed in the real space. This result implies that the complex space may provide a bypass between the initial and the optimal states even though they are both in the real space. On the other hand, Fig. 3(b) indicates that the worst 30% trials with the complex-space initialization had the slightly larger distance to the real space than the top 30% trials, which deteriorated the optimization. Figure 3(c) shows that the top 30% trials by FRAXIS converged in the real space while the worst 30% trials by FRAXIS got stuck with the significantly large distance to the real space. Compared to FQS and FRAXIS, we also observed that the distances to the real space were hardly changed during optimization by ROTOSELECT. Thus, the complex space did not bring benefits to the ROTOSELECT optimization, which implies that the continuous adjustment of the rotational axis, rather than the discrete one, is important to make use of the complex space for enhancing the trainability of PQC.

(b) Dependency of results on the number of layers. Next, we examined the dependency on the number of layers of PQCs. Here, we employed two kinds of PQCs: one is the alternating layered PQC in Fig. 1 and the other is the cascading block PQC in Fig. 4. The 30 independent trials for NFT, ROTOSELECT, FRAXIS, and FQS were performed for each condition. For ROTOSELECT and FQS, the complex-space initialization was used.

Figure 5 shows box plots of the relative errors of the objective function with respect to the exact minimum value for alternating layered and cascading block PQCs. As shown in Fig. 5(a), the benefits to use the complex search space were

conspicuous when the number of layers is relatively small while the converged objective function values obtained by FQS and NFT becomes closer as the number of layers becomes larger. This is because the expressibility of PQCs become high enough to express the solution even in the real space. Compared with FRAXIS, FQS led to better solutions, which implies that the simultaneous optimization of angles and axes of gates contributes to the efficient shortcut between the initial and the target states using the complex space. On the other hand, Fig. 5(b) shows that the objective function values converged by FQS, FRAXIS, and NFT exhibit no significant differences, which means that the effectiveness of the use of the complex space depends on PQCs. Therefore, we conclude that the continuously controllable angle and axis promotes the effective use of the complex space, which leads to higher-quality solutions especially with the shallow depth for a certain PQC structure. The feature of the PQC that can effectively bring out the benefits to use the complex space should be identified in the future research.

(c) Evaluation by the QASM simulator. Here, we examined the proposed method under finite-shot settings to study the effect of sampling errors by the QASM simulator in QISKIT [50]. To construct the matrices $S(\rho', A')$ and $S(\rho', B')$ in Eq. (17), we used the optimal parameter configuration, which can mitigate the sampling errors due to the geometrical symmetry of parameter configurations [41]. Although Ref. [41] obtained the optimal parameter configuration for eigenvalue problems, we confirmed that it is also applicable for generalized eigenvalue problems, as stated in Appendix F. We employed the alternating layered PQC in Fig. 1 with two layers. We used
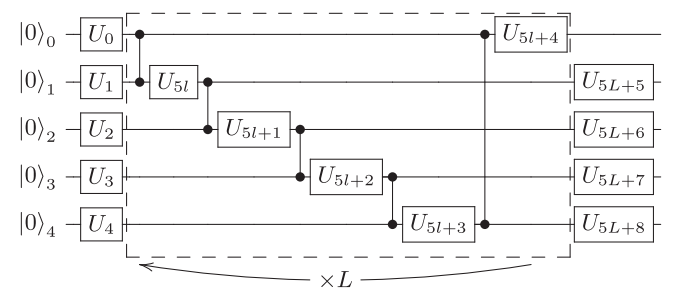

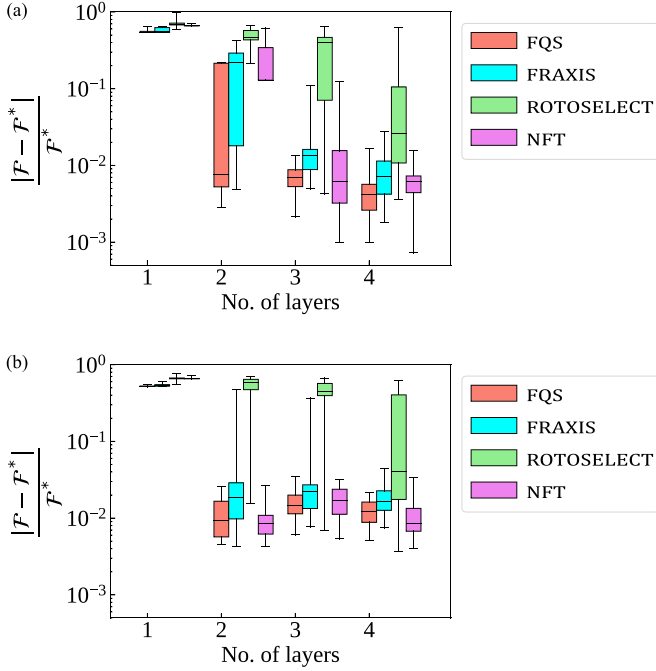FIG. 4. Cascading-block PQC for 5 qubits.

FIG. 5. Box plots of the relative error between the resulting objective function and the exact minimum value $\mathcal{F}^*$ for (a) alternating layered PQC and (b) Cascading block PQC. The 30 independent trials were performed for each setting of the number of layers.

the complex-space initialization for ROTOSELECT and FQS. We set the maximum number of iterations of the proposed method to 200 and performed the 10 independent trials for NFT, ROTOSELECT, FRAXIS, and FQS.

Figure 6 shows the history of the moving average of the maximum eigenvalue of Eq. (17) with the window length of 10. We observe the history became smoother as n_s increased. This history indicated that the result of FQS reaches larger eigenvalues than those of the other optimizers, which again demonstrated the benefits to use the complex search space.

We also observe that the maximum eigenvalues exceeded the exact optimal value shown by dashed-line several times. This would be because the eigenvalue whose matrix components are estimated by finite measurement outcomes includes the bias as discussed in Sec. III B. Figure 7 shows the history of the objective function value $\mathcal{F}$, which is reevaluated by the

state-vector simulator for the parameter history of each 10 independent trials in Fig. 6. As n_s increased, the errors between the estimated objective function value, i.e., the maximum eigenvalue in Fig. 6 and the actual objective function value in Fig. 7 became small. We also observed that the advantage of FQS over NFT was not distinct for $n_s = 10^4$. This would be because the effect of sampling errors on the objective function after parameter update in FQS is larger than that in NFT due to the larger difference between the maximum and minimum eigenvalues in FQS compared to NFT in Eq (21), which comes from that fact that the variational space of FQS includes that of NFT. That is, FQS has more potential to improve the objective function, but also has a susceptibility to sampling errors. In this study, we set the same number of shots to measure all quantum circuits for simplicity. We hope to conduct our future work to allocate the optimal number of shots for each quantum circuit to mitigate the sampling errors.

B. Eigenfrequency problem of a linear elastic solid

1. Problem statement

Next, let us consider the problem of finding the lowest eigenfrequency of a linear elastic solid, which is important in engineering to design mechanical structures for maximally improving their dynamic behaviors [56]. Because this application focuses on finding the lowest eigenfrequency that is obtained as the minimum of the objective function by the proposed method, one does not have to retrieve all the components of the optimized quantum state $|\psi(\{\boldsymbol{q}_d\})\rangle$.

Let $\Omega \subset \mathbb{R}^m$ denote an open bounded set where m is the number of spatial dimensions. The eigenvalue problem of a linear elastic solid occupying $\Omega \subset \mathbb{R}^m$ consists of the stress equilibrium equation, the constitutive law, and the displacement-strain relationship, which are respectively given as

$$\nabla \cdot \boldsymbol{\sigma}(\boldsymbol{x}) = -\varrho \omega^2 \boldsymbol{u}(\boldsymbol{x}),$$
$$\boldsymbol{\sigma}(\boldsymbol{x}) = \boldsymbol{C} : \boldsymbol{\varepsilon}(\boldsymbol{x}),$$
$$\boldsymbol{\varepsilon}(\boldsymbol{x}) = \tfrac{1}{2}(\nabla \boldsymbol{u} + \nabla \boldsymbol{u}^\top). \tag{33}$$

Here, $\boldsymbol{x} \in \Omega$ is the spatial coordinate, ϱ is the density of the solid, ω is the eigenfrequency, $\boldsymbol{u} \in \mathbb{R}^m$ is the displacement field, $\boldsymbol{\sigma}$ is the stress tensor, $\boldsymbol{C}$ is the elastic tensor, and $\boldsymbol{\varepsilon}$ is the strain tensor. The operator : represents the double-dot product, which acts as $\boldsymbol{C} : \boldsymbol{\varepsilon} = C_{ijkl}\varepsilon_{kl}$ with the Einstein's summation

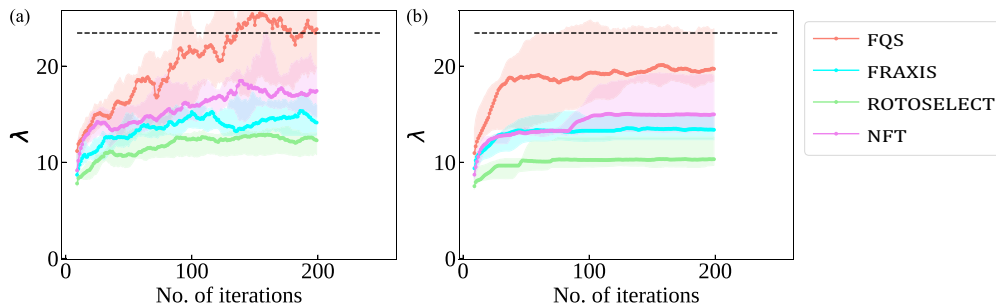FIG. 6. Histories of the moving average of the maximum eigenvalue of Eq. (17) with the window length of 10 for (a) $n_s = 10^4$ and (b) $n_s = 10^5$. n_s is the number of shots for individual quantum circuit. Plots represent the median value and shaded ranges represent ranges from 25- to 75-percentiles of the 10 independent trials. Dashed-line represents the exact optimal value of the objective function.
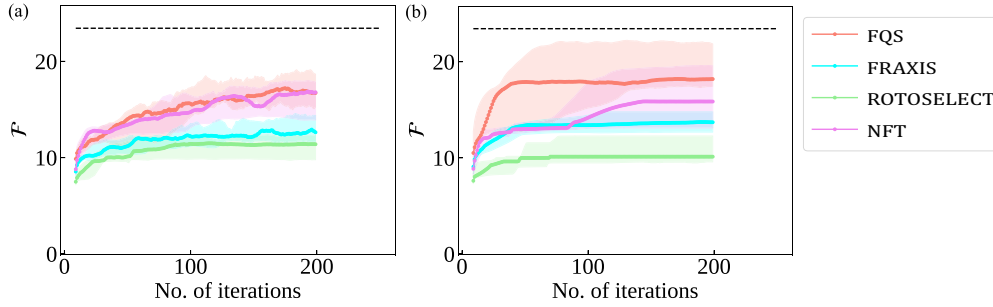
FIG. 7. Histories of the moving average of the objective function value $\mathcal{F}$ with the window length of 10, which is reevaluated by the state-vector simulator for the parameter history of each 10 independent trials in Figs. 6(a) and 6(b). Plots represent the median value and shaded ranges represent ranges from 25th to 75th percentiles of the 10 independent trials. Dashed line represents the exact optimal value of the objective function.

convention. Assuming that the solid is an isotropic material, the elastic tensor can be represented using the Young's modulus E and the Poisson ratio ν as

$$C_{ijkl} = \frac{E\nu}{(1+\nu)(1-2\nu)}\delta_{ij}\delta_{kl} + \frac{E}{2(1+\nu)}(\delta_{ik}\delta_{jl} + \delta_{il}\delta_{jk}),$$
(34)

where δ_{ij} is the Kronecker's delta. The Young's modulus represents the modulus of elasticity in tension or compression of a solid material. The Poisson ratio, which is in the range of $-1 < \nu < 0.5$, represents a measure of the deformation of a material in directions perpendicular to the specific direction of loading. These equations compose the governing equation of the displacement field $\boldsymbol{u}$. We consider that the Dirichlet boundary condition is imposed on the boundary $\Gamma_D \subset \partial\Omega$ as

$$\boldsymbol{u}(\boldsymbol{x}) = \boldsymbol{0} \quad \text{on } \boldsymbol{x} \in \Gamma_D.$$
(35)

Discretizing this governing equation by FEM [4,40] yields a GEP as follows:

$$KU = \lambda MU,$$
(36)

where $K \in \mathbb{R}^{(Nm)\times(Nm)}$ is the stiffness matrix, $M \in \mathbb{R}^{(Nm)\times(Nm)}$ is the mass matrix, $\boldsymbol{U} \in \mathbb{R}^{Nm}$ is the displacement field vector, and $\lambda = \omega^2$ is the eigenvalue. The discretization procedure by FEM is detailed in Appendix E 2. Both K and M are positive definite. Hence, the proposed method can be applied to analyzing the eigenfrequency of a linear elastic solid. In particular, $\text{tr}(B\rho) = \text{tr}(M\rho)$ and $\text{tr}(A\rho) = \text{tr}(K\rho)$ can be evaluated by XBM [44] as described before.

In this paper, we focus on the eigenvalue problem of a two-dimensional beam structure in the plain stress shown in Fig. 8. This beam structure is discretized using the first-order quadrilateral elements with $N_x \times N_y$ nodes where N_x is the number of nodes along the x axis and N_y is the number
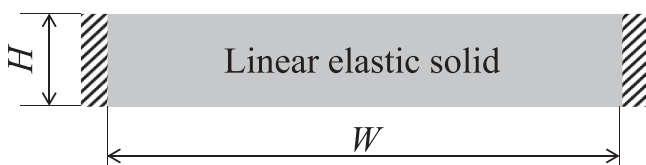
of nodes along the y axis. Since both sides are fixed, the number of degrees of freedom is $2(N_x - 2)N_y$, which results in the required number of qubits $n = \lceil\log_2(2(N_x - 2)N_y)\rceil = 1 + \lceil\log_2((N_x - 2)N_y)\rceil$. Here, we set $W = 1$, $H = 3/17$, $N_x = 18$, and $N_y = 4$, which leads to $n = 7$. The nodes of the finite elements are numbered from bottom left to top right in Fig. 9, and the binary representation of the node number is mapped to the computational basis of qubits. Note that the order of numbering and its mapping into qubits affect on the feasible solution generated by a PQC; this design problem is open for future work.

The Young's modulus and the Poisson ratio were, respectively, set to 200 GPa and 0.3. The material density ϱ was set to 7850 kg/m^3. These settings are typical for iron. Figure 9 illustrates the deformation mode corresponding to the ground state whose eigenvalue λ is 2.55×10^7 1/s^2 and the eigenfrequency $\omega/(2\pi) = \sqrt{\lambda}/(2\pi)$ is 8.04×10^2 Hz. Note that the solution, i.e., the displacement vector $\boldsymbol{u}$ of this problem, takes real values.

2. Results and discussion

Here, we employed the alternating layered PQC in Fig. 1 and used FQS, FRAXIS, and NFT. The 30 independent trials were performed for each method, and the complex-space initialization was used for FQS.

Figure 10 shows histories of the relative error of the objective function value $\mathcal{F}$ to the exact minimum value $\mathcal{F}^*$, which were obtained from independent 30 optimizations. To calculate the median and percentiles, we took the same statistical treatment as described in Sec. IV A 2. This figure indicates that half of trials of FQS and all trials of NFT and FRAXIS got stuck in poor local optima where the relative errors are larger
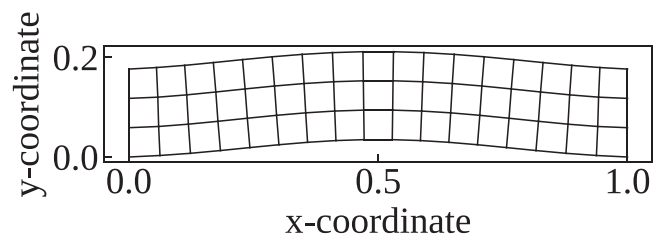

FIG. 8. Simulation model of a linear elastic solid. Both sides are fixed.

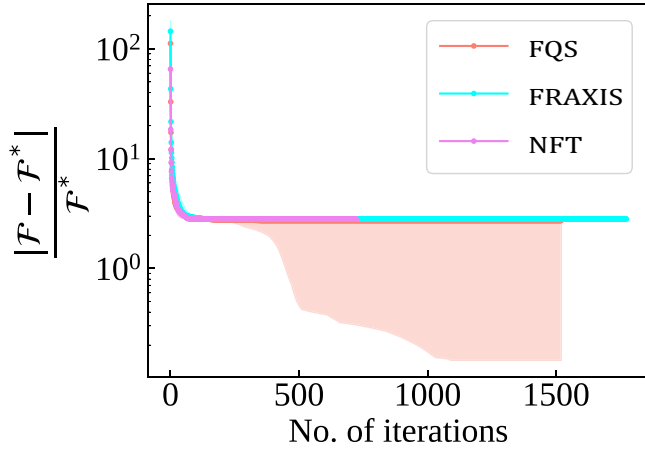FIG. 9. Deformation mode corresponding to the ground state.

FIG. 10. History of the relative error of the objective function value $\mathcal{F}$ to the exact minimum value $\mathcal{F}^*$. Plots represent the median value and shaded ranges represent ranges from 25th to 75th percentiles.

than 1. Nonetheless, the figure shows that the quarter of trials of FQS obtained much lower objective function values with the relative error of around 0.1. Thus, we again conclude that simultaneous and continuous optimization of angles and axes of gates is essential to fully exploiting the advantage to use the complex space. However, we actually observed that the many trials got stuck in poor local minima even when using this method (i.e., FQS with complex-valued initialization). We hope to address to construct a PQC structure which is suitable for such engineering problems in our future research.

V. CONCLUSIONS

This paper proposed a VQA for calculating the minimum or maximum eigenvalue of a GEP characterized by Hermitian matrices, based on sequential quantum optimization techniques. First, we formulated the GEP as the minimization problem of the generalized Rayleigh quotient, which is reformulated in the fractional form of the expectations of two Hermitians as the objective function of the VQA. We then showed that the objective function can be analytically minimized with respect to a single-qubit gate by solving GEP of a 4×4 matrix. Second, we showed that an SLE characterized by a positive-definite matrix can be formulated as a GEP and thus be attacked using the proposed method. Finally, we demonstrated applications to two important engineering problems formulated with FEM; one is for solving an SLE derived from a Poisson equation, and the other is eigenfrequency analysis of a linear elastic solid. Through the demonstration, we found that a problem having a real-valued solution can be solved more effectively using quantum gates generating a complex-valued state vector. There are several open problems including how to appropriately assign the ordering of optimization of single-qubit gates in PQC; to solve the eigenfrequency problem of a general elastic solid, how to suitably make numbering and mapping of finite-element nodes into qubits; how to construct a PQC suitable for exploiting the complex Hilbert space to efficiently solve real-valued engineering problems. Also, as

a future work we plan to determine an optimal number of shots for each quantum circuit for mitigating the sampling errors.

APPENDIX A: MINIMUM AND MAXIMUM OF RAYLEIGH QUOTIENT

Here, we consider to find $\boldsymbol{w}$ that minimizes or maximizes the generalized Rayleigh quotient $R(\boldsymbol{w}; A, B)$ in Eq. (2). The following theorem generalizes the previously known fact that holds when A and B are real-valued positive-definite matrices, e.g., see [2].

Theorem 1. Let $A \in \mathbb{C}^{N \times N}$ and $B \in \mathbb{C}^{N \times N}$ be a Hermitian and a positive-definite Hermitian, respectively, and let $(\lambda_{\min}, \boldsymbol{v}_{\min})$ and $(\lambda_{\max}, \boldsymbol{v}_{\max})$ denote the minimum and maximum eigenvalue-eigenvector pairs of the generalized eigenvalue problem $A\boldsymbol{v} = \lambda B\boldsymbol{v}$, respectively. Then, it holds that

$$\lambda_{\min}\boldsymbol{w}^\dagger B\boldsymbol{w} \leqslant \boldsymbol{w}^\dagger A\boldsymbol{w} \leqslant \lambda_{\max}\boldsymbol{w}^\dagger B\boldsymbol{w} \quad \forall \, \boldsymbol{w} \in \mathbb{C}^N, \quad \text{(A1)}$$

$$\lambda_{\min} = \min_{\boldsymbol{w}} R(\boldsymbol{w}; A, B) \text{ s.t. } \boldsymbol{w} \neq \boldsymbol{0}, \quad \text{(A2)}$$

$$\lambda_{\max} = \max_{\boldsymbol{w}} R(\boldsymbol{w}; A, B) \text{ s.t. } \boldsymbol{w} \neq \boldsymbol{0}, \quad \text{(A3)}$$

where $R(A, B; \boldsymbol{w})$ is the generalized Rayleigh quotient defined as

$$R(\boldsymbol{w}; A, B) := \frac{\boldsymbol{w}^\dagger A\boldsymbol{w}}{\boldsymbol{w}^\dagger B\boldsymbol{w}}. \quad \text{(A4)}$$

Proof. We first prove that Eq. (A1) holds by contradiction. Let us assume that $\boldsymbol{w}^\dagger A\boldsymbol{w} < \lambda_{\min}\boldsymbol{w}^\dagger B\boldsymbol{w}$. Then, it holds that

$$\boldsymbol{w}'^\dagger (B^{-1/2}AB^{-1/2} - \lambda_{\min}I)\boldsymbol{w}' < 0, \quad \text{(A5)}$$

where $\boldsymbol{w}' = B^{1/2}\boldsymbol{w}$, and it is ensured that $B^{1/2}$ and $B^{-1/2}$ exist because B is positive definite. Equation (A5) implies that the minimal eigenvalue of $B^{-1/2}AB^{-1/2}$ is lower than $\lambda_{\min}$. However, this contradicts that $\lambda_{\min}$ is the minimal eigenvalue because the eigenvalues of $B^{-1/2}AB^{-1/2}$ correspond to those of $A\boldsymbol{v} = \lambda B\boldsymbol{v}$, and consequently $\lambda_{\min}\boldsymbol{w}^\dagger B\boldsymbol{w} \leqslant \boldsymbol{w}^\dagger A\boldsymbol{w}$. Similarly, we obtain $\boldsymbol{w}^\dagger A\boldsymbol{w} \leqslant \lambda_{\max}\boldsymbol{w}^\dagger B\boldsymbol{w}$, which proves Eq. (A1).

Suppose $\boldsymbol{w} \neq \boldsymbol{0}$. Since B is positive definite, $\boldsymbol{w}^\dagger B\boldsymbol{w}$ is positive. Dividing Eq. (A1) by $\boldsymbol{w}^\dagger B\boldsymbol{w}$, we obtain

$$\lambda_{\min} \leqslant R(\boldsymbol{w}; A, B) \leqslant \lambda_{\max}. \quad \text{(A6)}$$

That is, the generalized Rayleigh quotient is bounded by $\lambda_{\min}$ and $\lambda_{\max}$. Furthermore, it holds that $\lambda_{\min} = R(\boldsymbol{v}_{\min}; A, B)$ and $\lambda_{\max} = R(\boldsymbol{v}_{\max}; A, B)$, which proved Eqs. (A2) and (A3). ∎

APPENDIX B: ENLARGEMENT OF MATRICES A AND B FOR THE n-QUBIT SYSTEM

Recall that we focus on a generalized eigenvalue problem (GEP) in Eq. (1) assuming $A \in \mathbb{C}^{N \times N}$ is a Hermitian matrix

and $B \in \mathbb{C}^{N \times N}$ is a positive-definite Hermitian matrix. The proposed method deals with the state vector of n-qubit system to represent the eigenvectors $\boldsymbol{v} \in \mathbb{C}^N$ of a GEP. When $\log_2 N$ is not an integer, we introduce enlarged matrices $\tilde{A} \in \mathbb{C}^{2^n \times 2^n}$ and $\tilde{B} \in \mathbb{C}^{2^n \times 2^n}$ to solve a GEP with the n-qubit system. In the following, we consider two cases depending on the eigenvalue of interest.

(a) When $\lambda_{\min} < 0$ or $\lambda_{\max} > 0$ is the eigenvalue of interest. We introduce the enlarged matrices $\tilde{A} \in \mathbb{C}^{2^n \times 2^n}$ and $\tilde{B} \in \mathbb{C}^{2^n \times 2^n}$ defined as

$$\tilde{A} := \begin{bmatrix} A & O_{N \times (2^n - N)} \\ O_{N \times (2^n - N)}^{\dagger} & O_{(2^n - N) \times (2^n - N)} \end{bmatrix}, \quad (B1)$$

$$\tilde{B} := \begin{bmatrix} B & O_{N \times (2^n - N)} \\ O_{N \times (2^n - N)}^{\dagger} & I_{(2^n - N) \times (2^n - N)} \end{bmatrix}, \quad (B2)$$

where $I_{(2^n - N) \times (2^n - N)}$ represents $(2^n - N) \times (2^n - N)$ identity matrix, and $O_{(2^n - N) \times (2^n - N)}$ and $O_{N \times (2^n - N)}$ represents $(2^n - N) \times (2^n - N)$ and $N \times (2^n - N)$ zero matrices, respectively. Considering the GEP expressed as

$$\tilde{A}\tilde{\boldsymbol{v}} = \lambda \tilde{B}\tilde{\boldsymbol{v}}, \quad (B3)$$

we obtain

$$\begin{aligned} A\boldsymbol{v} &= \lambda B\boldsymbol{v}, \\ \boldsymbol{0} &= \lambda \boldsymbol{v}', \end{aligned} \quad (B4)$$

where $\tilde{\boldsymbol{v}} = (\boldsymbol{v}^{\top}, \boldsymbol{v}'^{\top})^{\top}$. Equation (B4) means that the eigenvalues of the original GEP in Eq. (1) are also eigenvalues of Eq. (B3) with the corresponding eigenvectors $\tilde{\boldsymbol{v}} = (\boldsymbol{v}^{\top}, \boldsymbol{0}^{\top})^{\top}$. Additionally, $\lambda = 0$ is also an eigenvalue of Eq. (B3) where the corresponding eigenvector is $\tilde{\boldsymbol{v}} = (\boldsymbol{0}^{\top}, \boldsymbol{v}'^{\top})^{\top}$. When we are interested in the minimum eigenvalue $\lambda_{\min} < 0$ (the maximum eigenvalue $\lambda_{\max} > 0$) of the original GEP in Eq. (1), it is still the minimum (maximum) eigenvalue of the GEP in Eq. (B3). Therefore, we can minimize (maximize) the generalized Rayleigh quotient $R(\tilde{\boldsymbol{w}}; \tilde{A}, \tilde{B})$ where $\tilde{\boldsymbol{w}} \in \mathbb{C}^{2^n}$ can be represented by a state vector of n-qubit system.

(b) When $\lambda_{\min} > 0$ or $\lambda_{\max} < 0$ is the eigenvalue of interest.. We introduce the enlarged matrices $\tilde{A} \in \mathbb{C}^{2^n \times 2^n}$ and $\tilde{B} \in \mathbb{C}^{2^n \times 2^n}$ defined as

$$\tilde{A} := \begin{bmatrix} A & O_{N \times (2^n - N)} \\ O_{N \times (2^n - N)}^{\dagger} & I_{(2^n - N) \times (2^n - N)} \end{bmatrix}, \quad (B5)$$

$$\tilde{B} := \begin{bmatrix} B & O_{N \times (2^n - N)} \\ O_{N \times (2^n - N)}^{\dagger} & \epsilon I_{(2^n - N) \times (2^n - N)} \end{bmatrix}, \quad (B6)$$

where ϵ is a constant. Considering the GEP in Eq. (B3), we obtain

$$\begin{aligned} A\boldsymbol{v} &= \lambda B\boldsymbol{v}, \\ \boldsymbol{v}' &= \lambda \epsilon \boldsymbol{v}', \end{aligned} \quad (B7)$$

where $\tilde{\boldsymbol{v}} = (\boldsymbol{v}^{\top}, \boldsymbol{v}'^{\top})^{\top}$. Equation (B7) means that the eigenvalues of the original GEP in Eq. (1) are also eigenvalues of Eq. (B7) with the corresponding eigenvectors $\tilde{\boldsymbol{v}} = (\boldsymbol{v}^{\top}, \boldsymbol{0}^{\top})^{\top}$. Additionally, $\lambda = 1/\epsilon$ is also an eigenvalue of Eq. (B3) where the corresponding eigenvector is $\tilde{\boldsymbol{v}} = (\boldsymbol{0}^{\top}, \boldsymbol{v}'^{\top})^{\top}$. When we are interested in the minimum eigenvalue $\lambda_{\min} > 0$, a sufficiently small constant $\epsilon > 0$ keeps $\lambda_{\min}$ to be the minimum eigenvalue of GEP in Eq. (B3). In contrast, when we are interested in the maximum eigenvalue $\lambda_{\max} < 0$, a

negative constant $\epsilon < 0$ with a sufficiently small absolute value keeps $\lambda_{\max}$ to be the maximum eigenvalue of GEP in Eq. (B3). Therefore, we can minimize (maximize) the generalized Rayleigh quotient $R(\tilde{\boldsymbol{w}}; \tilde{A}, \tilde{B})$ where $\tilde{\boldsymbol{w}} \in \mathbb{C}^{2^n}$ can be represented by a state vector of n-qubit system.

APPENDIX C: ASYMPTOTIC BEHAVIOR OF EIGENVALUES UNDER SAMPLING ERRORS

The proposed method solves a small size GEP in Eq. (17) to update parameters in a PQC. Since the matrices $S(\rho', A')$ and $S(\rho', B')$ are constructed by expectation values of A and B calculated using several parameter sets, they will include the sampling errors, i.e., shot noises. Here, we analyze the asymptotic behavior of eigenvalues of Eq. (17).

Let S_A and S_B denote $S(\rho', A')$ and $S(\rho', B')$, respectively, for simple notations. Let n_s be the number of shots per individual quantum circuit for evaluating expectations of A and B. Since S_A and S_B are, respectively, constructed by the linear combination of expectation values of A and B calculated by several parameter sets, i.e., parameter configuration, the perturbations can be represented as

$$S_A = S_A^{(0)} + \epsilon S_A^{(1)}, \quad (C1)$$

$$S_B = S_B^{(0)} + \epsilon S_B^{(1)}, \quad (C2)$$

where ϵ is $O(1/\sqrt{n_s})$, the superscript (0) represents a quantity without any perturbation and (1) represents the first-order perturbation. Assuming that the expectation values of observable can be estimated unbiasedly, i.e., $\mathbb{E}[S_A] = S_A^{(0)}$ and $\mathbb{E}[S_B] = S_B^{(0)}$, we can suppose $\mathbb{E}[S_A^{(1)}] = \mathbb{E}[S_B^{(1)}] = O$ hold where O is a zero matrix. We now consider the asymptotic expansions of λ_i and $\boldsymbol{p}_i$ are, respectively, given as

$$\lambda_i = \lambda_i^{(0)} + \epsilon \lambda_i^{(1)} + \epsilon^2 \lambda_i^{(2)} + o(\epsilon^2), \quad (C3)$$

$$\boldsymbol{p}_i = \boldsymbol{p}_i^{(0)} + \epsilon \boldsymbol{p}_i^{(1)} + \epsilon^2 \boldsymbol{p}_i^{(2)} + o(\epsilon^2), \quad (C4)$$

where the superscript (2) represents the second-order perturbation. Substituting Eqs. (C1)–(C4) into Eq. (17), we obtain the following equations for each order of ϵ.

(a) $O(1)$ terms. These terms correspond to the GEP without any sampling errors and satisfy the equation given as

$$S_A^{(0)} \boldsymbol{p}_i^{(0)} = \lambda_i^{(0)} S_B^{(0)} \boldsymbol{p}_i^{(0)}. \quad (C5)$$

(b) $O(\epsilon)$ terms. We obtain the equation given as

$$S_A^{(0)} \boldsymbol{p}_i^{(1)} + S_A^{(1)} \boldsymbol{p}_i^{(0)} = \lambda_i^{(0)} S_B^{(0)} \boldsymbol{p}_i^{(1)} + \lambda_i^{(0)} S_B^{(1)} \boldsymbol{p}_i^{(0)} + \lambda_i^{(1)} S_B^{(0)} \boldsymbol{p}_i^{(0)}. \quad (C6)$$

Multiplying the above equation on the left by $\boldsymbol{p}_i^{(0)\top}$ and using Eq. (C5) and the normalized condition $\boldsymbol{p}_i^{(0)\top} S_B^{(0)} \boldsymbol{p}_i^{(0)} = 1$, we obtain

$$\lambda_i^{(1)} = \boldsymbol{p}_i^{(0)\top} (S_A^{(1)} - \lambda_i^{(0)} S_B^{(1)}) \boldsymbol{p}_i^{(0)}. \quad (C7)$$

Since $\mathbb{E}[S_A^{(1)}] = \mathbb{E}[S_B^{(1)}] = O$, the mean value of $\lambda_i^{(1)}$ is

$$\mathbb{E}[\lambda_i^{(1)}] = 0. \quad (C8)$$

(c) $O(\epsilon^2)$ terms. We obtain the equation as follows:

$$S_A^{(0)}\boldsymbol{p}_i^{(2)} + S_A^{(1)}\boldsymbol{p}_i^{(1)} = \lambda_i^{(0)}S_B^{(0)}\boldsymbol{p}_i^{(2)} + \lambda_i^{(0)}S_B^{(1)}\boldsymbol{p}_i^{(1)} + \lambda_i^{(1)}S_B^{(0)}\boldsymbol{p}_i^{(1)}$$
$$+ \lambda_i^{(1)}S_B^{(1)}\boldsymbol{p}_i^{(0)} + \lambda_i^{(2)}S_B^{(0)}\boldsymbol{p}_i^{(0)}. \quad (C9)$$

Multiplying the above equation on the left by $\boldsymbol{p}_i^{(0)\top}$ and rearranging the equations using Eqs. (C5) and (C6), and the normalized condition $\boldsymbol{p}_i^{(0)\top}S_B^{(0)}\boldsymbol{p}_i^{(0)} = 1$, we obtain

$$\lambda_i^{(2)} = -\lambda_i^{(1)}\boldsymbol{p}_i^{(0)\top}S_B^{(1)}\boldsymbol{p}_i^{(0)} - \boldsymbol{p}_i^{(1)\top}(S_A^{(0)} - \lambda_i^{(0)}S_B^{(0)})\boldsymbol{p}_i^{(1)}. \quad (C10)$$

Substituting Eq. (C7), we obtain the mean value of $\lambda_i^{(2)}$ as

$$\mathbb{E}[\lambda_i^{(2)}] = \lambda_i^{(0)}\mathbb{E}[(\boldsymbol{p}_i^{(0)\top}S_B^{(1)}\boldsymbol{p}_i^{(0)})^2]$$
$$- \mathbb{E}[\boldsymbol{p}_i^{(1)\top}(S_A^{(0)} - \lambda_i^{(0)}S_B^{(0)})\boldsymbol{p}_i^{(1)}]. \quad (C11)$$

These two terms in the right-hand side are not zero in general, and thus these appear as a bias of eigenvalues in Eq. (17), as follows:

$$\mathbb{E}[\lambda_i] = \lambda_i^{(0)} + \epsilon^2\lambda_i^{(0)}\mathbb{E}[(\boldsymbol{p}_i^{(0)\top}S_B^{(1)}\boldsymbol{p}_i^{(0)})^2]$$
$$- \epsilon^2\mathbb{E}[\boldsymbol{p}_i^{(1)\top}(S_A^{(0)} - \lambda_i^{(0)}S_B^{(0)})\boldsymbol{p}_i^{(1)}]. \quad (C12)$$

Therefore, the minimum (maximum) eigenvalue of Eq. (17) obtained with sampling errors is not an unbiased estimator of the optimal objective function value in Eq. (16) achievable by updating one single-qubit gate of interest. However, this bias vanishes asymptotically no slower than or equal to ϵ^2, i.e., $O(1/n_s)$.

Next, we estimate the actual objective function value after update of parameters using the perturbed eigenvector. Here, we consider the minimization of the objective function, but the maximization is straightforward. Substituting the perturbed eigenvector $\boldsymbol{p}_1$ into the objective function in Eq. (16), we obtain

$$\mathcal{F}(\boldsymbol{p}_1) = \frac{\boldsymbol{p}_1^\top S_A^{(0)}\boldsymbol{p}_1}{\boldsymbol{p}_1^\top S_B^{(0)}\boldsymbol{p}_1} \approx \frac{\boldsymbol{p}_1^{(0)\top}S_A^{(0)}\boldsymbol{p}_1^{(0)} + 2\epsilon\boldsymbol{p}_1^{(0)\top}S_A^{(0)}\boldsymbol{p}_1^{(1)} + \epsilon^2(2\boldsymbol{p}_1^{(0)\top}S_A^{(0)}\boldsymbol{p}_1^{(2)} + \boldsymbol{p}_1^{(1)\top}S_A^{(0)}\boldsymbol{p}_1^{(1)})}{\boldsymbol{p}_1^{(0)\top}S_B^{(0)}\boldsymbol{p}_1^{(0)} + 2\epsilon\boldsymbol{p}_1^{(0)\top}S_B^{(0)}\boldsymbol{p}_1^{(1)} + \epsilon^2(2\boldsymbol{p}_1^{(0)\top}S_B^{(0)}\boldsymbol{p}_1^{(2)} + \boldsymbol{p}_1^{(1)\top}S_B^{(0)}\boldsymbol{p}_1^{(1)})}$$
$$\approx \lambda_1^{(0)} + \epsilon^2\boldsymbol{p}_1^{(1)\top}(S_A^{(0)} - \lambda_1^{(0)}S_B^{(0)})\boldsymbol{p}_1^{(1)}. \quad (C13)$$

From the second to the third lines, we used the Taylor expansion with respect to ϵ up to the second order. Let $\boldsymbol{p}^{(1)}$ be expanded using the $\{\boldsymbol{p}_i^{(0)}\}$ as basis, as follows:

$$\boldsymbol{p}_1^{(1)} = \sum_j c_j \boldsymbol{p}_j^{(0)}, \quad (C14)$$

where c_j is a coefficient. Substituting this into Eq. (C13) and considering the normalization condition $\boldsymbol{p}_i^{(0)}S_B^{(0)}\boldsymbol{p}_j^{(0)} = \delta_{ij}$, we obtain

$$\mathcal{F}(\boldsymbol{p}_1) \approx \lambda_1^{(0)} + \epsilon^2\boldsymbol{p}_1^{(1)\top}(S_A^{(0)} - \lambda_1^{(0)}S_B^{(0)})\boldsymbol{p}_1^{(1)}$$
$$= \lambda_1^{(0)} + \epsilon^2\sum_j \|c_j\|^2(\lambda_j^{(0)} - \lambda_1^{(0)})$$
$$\leqslant \lambda_1^{(0)} + \epsilon^2(\lambda_{\max}^{(0)} - \lambda_1^{(0)})\sum_j \|c_j\|^2$$
$$= \lambda_1^{(0)} + \epsilon^2(\lambda_{\max}^{(0)} - \lambda_1^{(0)})\boldsymbol{p}_1^{(1)\top}S_B^{(0)}\boldsymbol{p}_1^{(1)}, \quad (C15)$$

where $\lambda_{\max}$ is the maximum eigenvalue. Therefore, the mean value of the objective function after parameter update is given as

$$\mathbb{E}[\mathcal{F}(\boldsymbol{p}_1)] \approx \lambda_1^{(0)} + \epsilon^2\mathbb{E}[\boldsymbol{p}_1^{(1)\top}(S_A^{(0)} - \lambda_1^{(0)}S_B^{(0)})\boldsymbol{p}_1^{(1)}]$$
$$\leqslant \lambda_1^{(0)} + \epsilon^2(\lambda_{\max}^{(0)} - \lambda_1^{(0)})\mathbb{E}[\boldsymbol{p}_1^{(1)\top}S_B^{(0)}\boldsymbol{p}_1^{(1)}], \quad (C16)$$

The second term is the gap between the ideal optimal value $\mathcal{F}(\boldsymbol{p}_1^{(0)}) = \lambda_1^{(0)}$ and the mean value of the actual value $\mathcal{F}(\boldsymbol{p}_1)$, and vanishes asymptotically no slower than or equal to ϵ^2.

APPENDIX D: OVERVIEW OF XBM

To evaluate the expectation value of an Hermitian H, i.e., $\langle H \rangle = \text{tr}(H\rho)$, this study employs the extended Bell measurement (XBM) [44]. Here, we briefly summarize the XBM. Let $A \in \mathbb{C}^{2^n \times 2^n}$ be the arbitrary matrix and A_{ij} the (i, j) component of A. In the XBM, the expectation value of A with the quantum state vector $|\psi\rangle \in \mathbb{C}^{2^n}$ is written as

$$\langle\psi|A|\psi\rangle = \sum_{i=0}^{2^n-1} A_{ii}|\langle i|\psi\rangle|^2 + \sum_{l \in \{i \oplus j|A_{ij}\neq 0\}\setminus\{0\}} \sum_{i=0}^{2^n-1}$$
$$\times \left(a_{\text{Re}}(A, l, i)|\langle i|M_{\text{Re}}^{(l)}|\psi\rangle|^2 + a_{\text{Im}}(A, l, i)\right.$$
$$\times \left.|\langle i|M_{\text{Im}}^{(l)}|\psi\rangle|^2\right), \quad (D1)$$

where $a_{\text{Re}}(A, l, i)$ and $a_{\text{Im}}(A, l, i)$ are the function of (A, l, i), and $M_{\text{Re}}^{(l)}$ and $M_{\text{Im}}^{(l)}$ are the measurement operators defined as

$$(M_{\text{Re}}^{(i\oplus j)})^\dagger|i\rangle = \frac{|i\rangle + |j\rangle}{\sqrt{2}},$$
$$(M_{\text{Im}}^{(i\oplus j)})^\dagger|i\rangle = \frac{|i\rangle + \iota|j\rangle}{\sqrt{2}}, \quad (D2)$$

respectively. Both measurement operators $M_{\text{Re}}^{(l)}$ and $M_{\text{Im}}^{(l)}$ can be expressed using at most one Hadamard gate, one phase gate, and $n - 1$ CNOT gates. It is known that when the bandwidth of A is $k = O(n^c)$ with a constant c, the number of groups for simultaneous measurement is $O(nk)$ [44].

APPENDIX E: MATRIX ASSEMBLY IN THE FINITE-ELEMENT METHOD [4,40]

Here, we briefly explain the matrix assembly in the finite-element method [4,40] to construct the stiffness matrix K for both the Poisson equation and the linear elastic solid, and the mass matrix M for the linear elastic solid. The main procedure is (1) deriving the weak form of the PDE to be solved, and (2) discretizing the weak form by introducing the shape function.

1. Assembly for the Poisson equation

First, let us derive the weak form of the Poisson equation in Eq. (27). Let $\tilde{u} \in H_0^1(\Omega)$ be an arbitrary function in the space $H_0^1(\Omega)$ defined as

$$H_0^1(\Omega) := \{\tilde{u} \in H^1(\Omega) \mid \tilde{u}(\boldsymbol{x}) = 0 \text{ on } \partial\Omega\}, \qquad \text{(E1)}$$

where $H^1(\Omega)$ is the Sobolev space. Multiplying Eq. (27) by the test function $\tilde{u}(\boldsymbol{x})$, and integrating both sides over the domain Ω, we obtain

$$-\int_\Omega \tilde{u}(\boldsymbol{x}) \nabla^2 u(\boldsymbol{x}) d\Omega = \int_\Omega \tilde{u}(\boldsymbol{x}) f(\boldsymbol{x}) d\Omega. \qquad \text{(E2)}$$

Applying the integration by parts and the Gauss's theorem to Eq. (E2), we derive the weak form of the Poisson equation as

$$\text{find} \quad u \in H_0^1(\Omega)$$

$$\text{s.t.} \int_\Omega \nabla\tilde{u}(\boldsymbol{x}) \cdot \nabla u(\boldsymbol{x}) d\Omega$$

$$= \int_\Omega \tilde{u}(\boldsymbol{x}) f(\boldsymbol{x}) d\Omega \ \forall \ \tilde{u} \in H_0^1(\Omega). \qquad \text{(E3)}$$

Next, we approximate the solution of the weak form by introducing the set of shape functions $\{\phi_j\}_{j=1}^N$ as $u(\boldsymbol{x}) \approx \sum_j \phi_j(\boldsymbol{x}) u_j$ and we set $\boldsymbol{U} := [u_1, \ldots u_N]^\top$. Substituting $u(\boldsymbol{x}) \approx \sum_j \phi_j(\boldsymbol{x}) u_j$ into the weak form in Eq. (E3) and taking $\tilde{u} = \phi_i$, we obtain

$$\sum_{j=1}^N u_j \int_\Omega \nabla\phi_i(\boldsymbol{x}) \cdot \nabla\phi_j(\boldsymbol{x}) d\Omega = \int_\Omega \phi_i(\boldsymbol{x}) f(\boldsymbol{x}) d\Omega. \qquad \text{(E4)}$$

Considering this equation in $i = 1, \ldots, N$ yields a linear system of the form

$$KU = F, \qquad \text{(E5)}$$

where

$$(K)_{ij} := \int_\Omega \nabla\phi_i(\boldsymbol{x}) \cdot \nabla\phi_j(\boldsymbol{x}) d\Omega, \qquad \text{(E6)}$$

$$(\boldsymbol{F})_i := \int_\Omega \phi_i(\boldsymbol{x}) f(\boldsymbol{x}) d\Omega. \qquad \text{(E7)}$$

Focusing on the case of one dimension, we consider the domain $\Omega = (0, 1)$ and introduce the uniform mesh

with nodes $0 < h = x_1 < x_2 < \cdots < x_N = 1 - h < 1$ where $x_{j+1} - x_j = h$ for all $j = 1, \ldots N - 1$. The first-order element we used employs the shape function ϕ_j defined as

$$\phi_j(x) = \begin{cases} 1 - \frac{|x-x_j|}{h} & \text{if } |x - x_j| \leqslant h, \\ 0 & \text{if } |x - x_j| > h. \end{cases} \qquad \text{(E8)}$$

Substituting Eq. (E8) into (E6) followed by a simple calculation shows that the stiffness matrix K is tridiagonal matrix written as

$$(K)_{ij} = \frac{1}{h} \begin{bmatrix} 2 & -1 & 0 & \cdots & 0 \\ -1 & 2 & -1 & \cdots & \\ & \ddots & \ddots & \ddots & \\ & & -1 & 2 & -1 \\ 0 & \cdots & 0 & -1 & 2 \end{bmatrix}. \qquad \text{(E9)}$$

To obtain the vector $\boldsymbol{F}$, we can use a certain quadrature formula to calculate the integration of the right-hand side of Eq. (E7). In this study, we take $(\boldsymbol{F})_j = f(x_j)$, for simplicity.

2. Assembly for the eigenvalue problem of a linear elastic solid

We proceed in a similar manner to the discretization of the Poisson equation in Appendix E 1 to obtain the stiffness matrix K and the mass matrix M for the eigenfrequency analysis of a linear elastic solid by the finite-element method [4,40]. By a similar procedure to the case of the Poisson equation, we obtain the weak form of Eq. (33) as

$$\text{find} \quad \boldsymbol{u} \in \mathcal{U}$$

$$\text{s.t.} \int_\Omega \tilde{\boldsymbol{\varepsilon}} : \boldsymbol{C} : \boldsymbol{\varepsilon} \, d\Omega$$

$$= \int_\Omega \varrho\omega^2 \tilde{\boldsymbol{u}} \cdot \boldsymbol{u} \, d\Omega \quad \forall \ \tilde{\boldsymbol{u}} \in \mathcal{U}, \qquad \text{(E10)}$$

where ϱ is the density of the solid,

$$\boldsymbol{\varepsilon}(\boldsymbol{x}) = \tfrac{1}{2}(\nabla\boldsymbol{u} + \nabla\boldsymbol{u}^\top), \qquad \text{(E11)}$$

$$\tilde{\boldsymbol{\varepsilon}}(\boldsymbol{x}) = \tfrac{1}{2}(\nabla\tilde{\boldsymbol{u}} + \nabla\tilde{\boldsymbol{u}}^\top), \qquad \text{(E12)}$$

and $\mathcal{U}$ is the Sobolev space defined as

$$\mathcal{U} := \{\boldsymbol{u} \in H^1(\Omega)^m \mid \boldsymbol{u}(\boldsymbol{x}) = 0 \text{ on } \Gamma_\mathrm{D}\}. \qquad \text{(E13)}$$

$\Gamma_\mathrm{D} \subset \partial\Omega$ is the boundary on which the displacement $\boldsymbol{u}$ is fixed.

We now consider to approximate the solution of the weak form by using the shape functions, i.e., $\boldsymbol{u}(\boldsymbol{x}) \approx \sum_j \phi_j(\boldsymbol{x}) \boldsymbol{u}_j$ and we set $\boldsymbol{U} := [\boldsymbol{u}_1^\top, \ldots, \boldsymbol{u}_N^\top]^\top$ which has the dimension of Nm since the solution $\boldsymbol{u}$ is a vector-valued function that takes values in $\mathbb{R}^m$. That is, the $[m(j-1) + l]$th component of $\boldsymbol{U}$ represents the displacement at jth node along the lth axis, i.e., $(\boldsymbol{u}_j)_l$. Substituting $\boldsymbol{u} \approx \sum_j \phi_j(\boldsymbol{x}) \boldsymbol{u}_j$ and Eq. (34) into Eq. (E10) and taking $(\tilde{\boldsymbol{u}})_{k'} = \delta_{kk'}\phi_i$, we obtain

$$\sum_{j,l}(\boldsymbol{u}_j)_l \int_\Omega \left(\frac{E\nu}{(1+\nu)(1-2\nu)}\phi_{i,k}(\boldsymbol{x})\phi_{j,l}(\boldsymbol{x}) + \frac{E}{2(1+\nu)}\delta_{kl}\nabla\phi_i(\boldsymbol{x}) \cdot \nabla\phi_j(\boldsymbol{x}) + \frac{E}{2(1+\nu)}\phi_{j,k}\phi_{i,l} \right) d\Omega$$

$$= \lambda \sum_{j,l}(\boldsymbol{u}_j)_l \int_\Omega \varrho\delta_{kl}\phi_i(\boldsymbol{x})\phi_j(\boldsymbol{x}) d\Omega, \qquad \text{(E14)}$$

where $\lambda = \omega^2$ and $\phi_{\alpha,\beta}$ represents $\partial\phi_\alpha/\partial x_\beta$. Considering Eq. (E14) in $i = 1, \ldots, N$ and $k = 1 \ldots, m$ yields a generalized eigenvalue problem of the form

$$KU = \lambda MU, \tag{E15}$$

where

$$(K)_{i'j'} := \int_\Omega \left(\frac{E\nu}{(1+\nu)(1-2\nu)}\phi_{i,k}(\boldsymbol{x})\phi_{j,l}(\boldsymbol{x}) + \frac{E}{2(1+\nu)}\delta_{kl}\boldsymbol{\nabla}\phi_i(\boldsymbol{x})\cdot\boldsymbol{\nabla}\phi_j(\boldsymbol{x}) + \frac{E}{2(1+\nu)}\phi_{j,k}\phi_{i,l} \right)d\Omega, \tag{E16}$$

$$(M)_{i'j'} := \int_\Omega \varrho\delta_{kl}\phi_i(\boldsymbol{x})\phi_j(\boldsymbol{x})d\Omega, \tag{E17}$$

using the notation $i' := m(i-1) + k$ and $j' := m(j-1) + l$.

Focusing on the case of two dimensions, we consider the domain $\Omega = (0, W) \times (0, H)$ and introduce the grid mesh with nodes (x_{j_x}, y_{j_y}) defined by the equally spaced points along each axis, $0 = x_1 < x_2 < \cdots < x_{N_x} = W$ and $0 = y_1 < y_2 < \cdots < y_{N_y} = H$ where $x_{j_x+1} - x_{j_x} = h_x$ for all $j_x = 1, \ldots N_x - 1$ and $y_{j_y+1} - y_{j_y} = h_y$ for all $j_y = 1, \ldots N_y - 1$, respectively. We used the first-order element which employs the shape function ϕ_j defined as

$$\phi_j(x, y) = \begin{cases} \left(1 - \frac{|x-x_{j_x}|}{h_x}\right)\left(1 - \frac{|y-y_{j_y}|}{h_y}\right) & \text{if } |x - x_{j_x}| \leqslant h_x \text{ and } |y - y_{j_y}| \leqslant h_y, \\ 0 & \text{otherwise,} \end{cases} \tag{E18}$$

associating j with j_x and j_y as $j = N_y(j_x - 1) + j_y$. We used the Gauss quadrature rule for calculating the integration.

APPENDIX F: OPTIMAL PARAMETER CONFIGURATION FOR GENERALIZED EIGENVALUE PROBLEM

In the following, we consider the minimization of the objective function, the minimum eigenvalue of Eq. (17). The analysis for the maximization problems is straightforward. Let $P := \{\tilde{\boldsymbol{q}}_i\}_{i=1}^r$ be the parameter configuration, the set of r parameters, and $\boldsymbol{h}_A := (h_{A1}, \ldots, h_{Ar})^\top$ and $\boldsymbol{h}_B := (h_{B1}, \ldots, h_{Br})^\top$ be the expectation values of A and B through the parameter in the configuration. Typically, $r = 10$ for FQS, $r = 6$ for FRAXIS, and $r = 3$ for NFT. Let S_A and S_B denote $S(\rho', A')$ and $S(\rho', B')$, respectively, for simple notations. Since S_A and S_B are, respectively, constructed by applying the linear transformation depending on the parameter configuration to $\boldsymbol{h}_A$ and $\boldsymbol{h}_B$ [41], S_A and S_B are represented as

$$S_A = T(\boldsymbol{h}_A|P), \tag{F1}$$

$$S_B = T(\boldsymbol{h}_B|P), \tag{F2}$$

where T is the linear transformation depending of the parameter configuration P. Now, we assume that the expectation values are perturbed due to sampling errors around $\boldsymbol{h}_A$ and $\boldsymbol{h}_B$ by uncorrelated Gaussian noises $\boldsymbol{\delta}_A \sim \mathcal{N}(\boldsymbol{0}, \sigma_A^2/n_s I)$ and $\boldsymbol{\delta}_B \sim \mathcal{N}(\boldsymbol{0}, \sigma_B^2/n_s I)$, respectively, where σ_A^2 and σ_B^2 are the variances of estimating each entry of $\boldsymbol{h}_A$ and $\boldsymbol{h}_B$, respectively, and I is the $r \times r$ identity matrix. Note that the variances of each entry of $\boldsymbol{h}_A$ and $\boldsymbol{h}_B$ are not in general the same since they depend on parameters of PQC. However, we herein as-

sume the variances are the same to discuss the parameter configuration independent from particular parameter values of PQC. The assumption of the uncorrelated Gaussian noises correspond to the assumption that the estimation of the expectation values of A and B is unbiased, i.e., $\mathbb{E}[\boldsymbol{\delta}_A] = \mathbb{E}[\boldsymbol{\delta}_B] = \boldsymbol{0}$ and that the measurement outcomes of quantum circuits are independent, i.e., $\mathbb{E}[\delta_{Ai}\delta_{Aj}] = \mathbb{E}[\delta_{Bi}\delta_{Bj}] = \mathbb{E}[\delta_{Ai}\delta_{Bj}] = 0$ for $i, j(\neq i) \in \{1, \ldots, r\}$. Under sampling errors, S_A and S_B are now represented as

$$S_A = T(\boldsymbol{h}_A|P) + T(\boldsymbol{\delta}_A|P), \tag{F3}$$

$$S_B = T(\boldsymbol{h}_B|P) + T(\boldsymbol{\delta}_B|P). \tag{F4}$$

That is, $T(\boldsymbol{h}_A|P)$ and $T(\boldsymbol{h}_B|P)$ correspond to $S(\rho', A')^{(0)}$ and $S(\rho', B')^{(0)}$, respectively, and $T(\boldsymbol{\delta}_A|P)$ and $T(\boldsymbol{\delta}_B|P)$ correspond to $\epsilon S(\rho', A')^{(1)}$ and $\epsilon S(\rho', B')^{(1)}$, respectively. To derive the optimal parameter configuration, we focus on the variance of the minimum eigenvalue in Eq. (17). The smaller the variance of the eigenvalue is, the more accurately the objective function value is estimated under the sampling errors. Based on the first-order perturbation, the variance of the minimum eigenvalue is given as

$$\text{Var}[\lambda_1] = \text{Var}\big[\boldsymbol{p}_i^{(0)\top} T\big(\boldsymbol{\delta}_A - \lambda_1^{(0)}\boldsymbol{\delta}_B|P\big)\boldsymbol{p}_i^{(0)}\big]. \tag{F5}$$

To minimize $\text{Var}[\lambda_1]$ with respect to P, we can use the same analysis as that in Ref. [41], assuming that $\boldsymbol{\delta}_A - \lambda_1^{(0)}\boldsymbol{\delta}_B$ follows the uncorrelated Gaussian distribution, which is actually satisfied from the assumption of $\boldsymbol{\delta}_A$ and $\boldsymbol{\delta}_B$. Thus, we can evaluate Eq. (9) using the optimal parameter configuration, which is the set of parameters aligned in a symmetric manner, to mitigate the sampling errors.

[1] D. Boffi, Finite element approximation of eigenvalue problems, Acta Numerica **19**, 1 (2010).

[2] S. Yu, L.-C. Tranchevent, B. De Moor, and Y. Moreau, Kernel-based data fusion for machine learning, in *Studies in Computational Intelligence* (Springer, Berlin, 2011).

[3] B. Ford and G. Hall, The generalized eigenvalue problem in quantum chemistry, Comput. Phys. Commun. **8**, 337 (1974).

[4] T. J. Hughes, *The Finite Element Method: Linear Static and Dynamic Finite Element Analysis* (Dover, New York, 2012).

[5] A. Klawonn, M. Lanser, and O. Rheinbach, Toward extremely scalable nonlinear domain decomposition methods for elliptic partial differential equations, SIAM J. Sci. Comput. **37**, C667 (2015).

[6] J. Toivanen, P. Avery, and C. Farhat, A multilevel FETI-DP method and its performance for problems with billions of degrees of freedom, Int. J. Numer. Methods Eng. **116**, 661 (2018).

[7] A. Aspuru-Guzik, A. D. Dutoi, P. J. Love, and M. Head-Gordon, Simulated quantum computation of molecular energies, Science **309**, 1704 (2005).

[8] P. J. J. O'Malley, R. Babbush, I. D. Kivlichan, J. Romero, J. R. McClean, R. Barends, J. Kelly, P. Roushan, A. Tranter, N. Ding *et al.*, Scalable Quantum Simulation of Molecular Energies, Phys. Rev. X **6**, 031007 (2016).

[9] J. B. Parker and I. Joseph, Quantum phase estimation for a class of generalized eigenvalue problems, Phys. Rev. A **102**, 022422 (2020).

[10] A. Peruzzo, J. McClean, P. Shadbolt, M.-H. Yung, X.-Q. Zhou, P. J. Love, A. Aspuru-Guzik, and J. L. O'Brien, A variational eigenvalue solver on a photonic quantum processor, Nat. Commun. **5**, 4213 (2014).

[11] A. Kandala, A. Mezzacapo, K. Temme, M. Takita, M. Brink, J. M. Chow, and J. M. Gambetta, Hardware-efficient variational quantum eigensolver for small molecules and quantum magnets, Nature (London) **549**, 242 (2017).

[12] Y. Li, J. Hu, X.-M. Zhang, Z. Song, and M.-H. Yung, Variational quantum simulation for quantum chemistry, Adv. Theory Simul. **2**, 1800182 (2019).

[13] F. Zhang, N. Gomes, N. F. Berthusen, P. P. Orth, C.-Z. Wang, K.-M. Ho, and Y.-X. Yao, Shallow-circuit variational quantum eigensolver based on symmetry-inspired hilbert space partitioning for quantum chemical calculations, Phys. Rev. Res. **3**, 013039 (2021).

[14] M. Cerezo, A. Arrasmith, R. Babbush, S. C. Benjamin, S. Endo, K. Fujii, J. R. McClean, K. Mitarai, X. Yuan, L. Cincio *et al.*, Variational quantum algorithms, Nat. Rev. Phys. **3**, 625 (2021).

[15] J. Tilly, H. Chen, S. Cao, D. Picozzi, K. Setia, Y. Li, E. Grant, L. Wossnig, I. Rungger, G. H. Booth, and J. Tennyson, The variational quantum eigensolver: A review of methods and best practices, Phys. Rep. **986**, 1 (2022).

[16] N. Gomes, A. Mukherjee, F. Zhang, T. Iadecola, C.-Z. Wang, K.-M. Ho, P. P. Orth, and Y.-X. Yao, Adaptive variational quantum imaginary time evolution approach for ground state preparation, Adv. Quantum Technol. **4**, 2100114 (2021).

[17] O. Higgott, D. Wang, and S. Brierley, Variational quantum computation of excited states, Quantum **3**, 156 (2019).

[18] K. M. Nakanishi, K. Mitarai, and K. Fujii, Subspace-search variational quantum eigensolver for excited states, Phys. Rev. Res. **1**, 033062 (2019).

[19] S. Gocho, H. Nakamura, S. Kanno, Q. Gao, T. Kobayashi, T. Inagaki, and M. Hatanaka, Excited state calculations using variational quantum eigensolver with spin-restricted ansätze and automatically-adjusted constraints, npj Comput. Mater. **9**, 13 (2023).

[20] H. Hirai, Excited-state molecular dynamics simulation based on variational quantum algorithms, Chem. Phys. Lett. **816**, 140404 (2023).

[21] M. Benedetti, M. Fiorentini, and M. Lubasch, Hardware-efficient variational quantum algorithms for time evolution, Phys. Rev. Res. **3**, 033083 (2021).

[22] K. Wada, R. Raymond, Yu-ya Ohnishi, E. Kaminishi, M. Sugawara, N. Yamamoto, and H. C. Watanabe, Simulating time evolution with fully optimized single-qubit gates on parametrized quantum circuits, Phys. Rev. A **105**, 062421 (2022).

[23] H.-L. Liu, Y.-S. Wu, L.-C. Wan, S.-J. Pan, S.-J. Qin, F. Gao, and Q.-Y. Wen, Variational quantum algorithm for the poisson equation, Phys. Rev. A **104**, 022418 (2021).

[24] Y. Sato, R. Kondo, S. Koide, H. Takamatsu, and N. Imoto, Variational quantum algorithm based on the minimum potential energy for solving the poisson equation, Phys. Rev. A **104**, 052409 (2021).

[25] R. Demirdjian, D. Gunlycke, C. A. Reynolds, J. D. Doyle, and S. Tafur, Variational quantum solutions to the advection–diffusion equation for applications in fluid dynamics, Quantum Inf. Proc. **21**, 322 (2022).

[26] C. Bravo-Prieto, R. LaRose, M. Cerezo, Y. Subasi, L. Cincio, and P. J. Coles, Variational quantum linear solver, arXiv:1909.05820.

[27] X. Xu, J. Sun, S. Endo, Y. Li, S. C. Benjamin, and X. Yuan, Variational algorithms for linear algebra, Sci. Bull. **66**, 2181 (2021).

[28] R. LaRose, A. Tikku, É. O'Neel-Judy, L. Cincio, and P. J. Coles, Variational quantum state diagonalization, npj Quantum Inf. **5**, 57 (2019).

[29] M. Cerezo, K. Sharma, A. Arrasmith, and P. J. Coles, Variational quantum state eigensolver, npj Quantum Inf. **8**, 113 (2022).

[30] J.-M. Liang, S.-Q. Shen, M. Li, and L. Li, Variational quantum algorithms for dimensionality reduction and classification, Phys. Rev. A **101**, 032323 (2020).

[31] J.-M. Liang, S.-Q. Shen, M. Li, and S.-M. Fei, Quantum algorithms for the generalized eigenvalue problem, Quantum Inf. Proc. **21**, 23 (2022).

[32] K. M. Nakanishi, K. Fujii, and S. Todo, Sequential minimal optimization for quantum-classical hybrid algorithms, Phys. Rev. Res. **2**, 043158 (2020).

[33] M. Ostaszewski, E. Grant, and M. Benedetti, Structure optimization for parameterized quantum circuits, Quantum **5**, 391 (2021).

[34] H. C. Watanabe, R. Raymond, Yu-Ya Ohnishi, E. Kaminishi, and M. Sugawara, Optimizing parameterized quantum circuits with free-axis selection, in *Proceedings of the 2021 IEEE International Conference on Quantum Computing and Engineering (QCE)* (IEEE, Piscataway, NJ, 2021), pp 100–111.

[35] K. Wada, R. Raymond, Y. Sato, and H. C. Watanabe, Sequential optimal selection of a single-qubit gate and its relation to barren plateau in parameterized quantum circuits, arXiv:2209.08535.

[36] L. C. Evans, *Partial Differential Equations* (American Mathematical Society, Providence, RI, 2010), Vol. 19.

[37] M. Peter Deisenroth, A. A. Faisal, and C. S. Ong, *Mathematics for Machine Learning* (Cambridge University Press, Cambridge, 2020).

[38] C. C. Aggarwal, L.-F. Aggarwal, and Lagerstrom-Fife, *Linear Algebra and Optimization for Machine Learning* (Springer, Berlin, 2020), Vol. 156.

[39] Y. Y. Liu, Z. Chen, C. Shu, S.-C. Chew, B. C. Khoo, X. Zhao, and Y. D. Cui, Application of a variational hybrid quantum-classical algorithm to heat conduction equation and analysis of time complexity, Phys. Fluids **34**, 117121 (2022).

[40] G. Allaire, *Numerical Analysis and Optimization: An Introduction to Mathematical Modelling and Numerical Simulation* (Oxford University Press, Oxford, 2007).

[41] K. Endo, Y. Sato, R. Raymond, K. Wada, N. Yamamoto, and H. C. Watanabe, Optimal parameter configurations for sequential optimization of variational quantum eigensolver, arXiv:2303.07082.

[42] G. Cardano, *Ars Magna or The Rules of Algebra* (Dover, New York, 1993).

[43] A. W. Harrow, A. Hassidim, and S. Lloyd, Quantum Algorithm for Linear Systems of Equations, Phys. Rev. Lett. **103**, 150502 (2009).

[44] R. Kondo, Y. Sato, S. Koide, S. Kajita, and H. Takamatsu, Computationally efficient quantum expectation with extended bell measurements, Quantum **6**, 688 (2022).

[45] D. Ribeiro, R. Calçada, R. Delgado, M. Brehm, and V. Zabel, Finite-element model calibration of a railway vehicle based on experimental modal parameters, Vehicle Syst. Dynam. **51**, 821 (2013).

[46] A. Muhammad, M. A. H. Ali, and I. H. Shanono, Finite element analysis of a connecting rod in ANSYS: An overview, in *IOP Conference Series: Materials Science and Engineering, Volume 736, Engineering Science and Technology* (IOP Publishing, Bristol, 2020), p. 022119.

[47] A. Belhocine and O. Ibraheem Abdullah, Thermomechanical model for the analysis of disc brake using the finite element method in frictional contact, Multiscale Sci. Eng. **2**, 27 (2020).

[48] X.-M. Zhang, M.-H. Yung, and X. Yuan, Low-depth quantum state preparation, Phys. Rev. Res. **3**, 043200 (2021).

[49] K. Nakaji, S. Uno, Y. Suzuki, R. Raymond, T. Onodera, T. Tanaka, H. Tezuka, N. Mitsuda, and N. Yamamoto, Approximate amplitude encoding in shallow parameterized quantum circuits and its application to financial market indicators, Phys. Rev. Res. **4**, 023136 (2022).

[50] H. Abraham *et al.*, Qiskit contributors, Qiskit: An Open-source Framework for Quantum Computing (2023), https://qiskit.org/documentation/faq.html.

[51] D. J. Griffiths, *Introduction to Electrodynamics* (Cambridge University Press, Cambridge, 1999).

[52] T. J. Chung, *Computational Fluid Dynamics* (Cambridge University Press, Cambridge, 2010).

[53] J. Blazek, *Computational Fluid Dynamics: Principles and Applications* (Butterworth-Heinemann, Oxford, 2015).

[54] Y. Ruan, X. Xue, and Y. Shen, Quantum image processing: opportunities and challenges, Math. Probl. Eng. **2021**, 6671613 (2021).

[55] M. Cerezo, A. Sone, T. Volkoff, L. Cincio, and P. J. Coles, Cost function dependent barren plateaus in shallow parametrized quantum circuits, Nat. Commun. **12**, 1791 (2021).

[56] Z.-D. Ma, H.-C. Cheng, and N. Kikuchi, Structural design for obtaining desired eigenfrequencies by using the topology and shape optimization method, Comput. Syst. Eng. **5**, 77 (1994).